the plant journal

SEB SOCIETY FOR EXPERIMENTAL BIOLOGY

The Plant Journal (2023) **113,** 1330–1347 doi: 10.1111/tpj.16113

Pine has two glutamine synthetase paralogs, GS1b.1 and GS1b.2, exhibiting distinct biochemical properties

José Miguel Valderrama-Martín[1,2], Francisco Ortigosa[1], Juan Carlos Aledo[2], Concepción Ávila[1], Francisco M. Cánovas[1] and Rafael A. Cañas[2,*]

[1]*Grupo de Biología Molecular y Biotecnología, Departamento de Biología Molecular y Bioquímica, Universidad de Málaga, Campus Universitario de Teatinos, 29071, Málaga, Spain, and*

[2]*Integrative Molecular Biology Lab, Universidad de Málaga, Campus Universitario de Teatinos, 29071, Málaga, Spain*

Received 2 November 2022; revised 15 December 2022; accepted 13 January 2023; published online 19 January 2023.
*For correspondence (e-mail rcanas@uma.es)

SUMMARY

The enzyme glutamine synthetase (EC 6.3.1.2) is mainly responsible for the incorporation of inorganic nitrogen into organic molecules in plants. In the present work, a pine (*Pinus pinaster*) *GS1* (*PpGS1b.2*) gene was identified, showing a high sequence identity with the *GS1b.1* gene previously characterized in conifers. Phylogenetic analysis revealed that the presence of *PpGS1b.2* is restricted to the genera *Pinus* and *Picea* and is not found in other conifers. Gene expression data suggest a putative role of *PpGS1b.2* in plant development, similar to other *GS1b* genes from angiosperms, suggesting evolutionary convergence. The characterization of GS1b.1 and GS1b.2 at the structural, physicochemical, and kinetic levels has shown differences even though they have high sequence homology. GS1b.2 had a lower optimum pH (6 vs. 6.5) and was less thermally stable than GS1b.1. GS1b.2 exhibited positive cooperativity for glutamate and substrate inhibition for ammonium. However, GS1b.1 exhibited substrate inhibition behavior for glutamate and ATP. Alterations in the kinetic characteristics produced by site-directed mutagenesis carried out in this work strongly suggest an implication of amino acids at positions 264 and 267 in the active center of pine GS1b.1 and GS1b.2 being involved in affinity toward ammonium. Therefore, the amino acid differences between GS1b.1 and GS1b.2 would support the functioning of both enzymes to meet distinct plant needs.

Keywords: biochemistry, development, glutamine synthetase, kinetic parameters, nitrogen metabolism, physicochemical properties, conifer, *Pinus pinaster*.

INTRODUCTION

Nitrogen (N) is an essential element, a constituent of the main biomolecules, and a limiting factor for plant growth (Hirel & Krapp, 2021). N is assimilated from ammonium into organic molecules by the glutamine synthetase (GS, EC 6.3.1.2)/glutamate synthase (GOGAT, EC 1.4.7.1) cycle. Ammonium is first incorporated into glutamate to form glutamine in an ATP-dependent reaction catalyzed by GS (Heldt & Piechulla, 2011), and then this glutamine together with 2-oxoglutarate is used to produce two glutamate molecules by GOGAT (Bernard & Habash, 2009). Studies have shown that up to 95% of ammonium is assimilated via the GS/GOGAT cycle (Lea & Ireland, 1999) for the formation of glutamine and glutamate, which, in turn, will be used to produce all N-containing biomolecules in the plant (Bernard & Habash, 2009; Forde & Lea, 2007).

GS has been widely studied in plants since it is directly responsible for the incorporation of inorganic N into organic molecules. Recently, three different lineages of *GS* genes have been identified in seed plants: *GS1a* and *GS1b* encode cytosolic enzymes, and *GS2* encodes a plastid-located enzyme (Valderrama-Martín et al., 2022). The three *GS* gene lineages are present in cycads and ginkgo (*Ginkgo biloba*), as well as basal angiosperms. Nevertheless, no *GS2* genes have been found in other gymnosperms, such as conifers and gnetales, and no *GS1a* genes have been found in modern angiosperms, including monocot and eudicot species (Valderrama-Martín et al., 2022). In general, GS1b is encoded by a small multigene family, while GS1a and GS2 are usually encoded by a single nuclear gene (James et al., 2018; Valderrama-Martín et al., 2022).

GS2 and GS1a are associated with photosynthetic organs (Ávila et al., 2001; Blackwell et al., 1987), and their expression is regulated by light conditions (Cantón et al., 1999; Gómez-Maldonado, Ávila, et al., 2004;

Valderrama-Martín et al., 2022). Indeed, GS2 and GS1a are considered to play a fundamental role in the assimilation of the ammonium released during photorespiration and nitrate photoassimilation processes (Blackwell et al., 1987; Cantón et al., 1999; Tegeder & Masclaux-Daubresse, 2017; Wallsgrove et al., 1987). In this sense, new evidence suggests that the *GS2* gene may have arisen through duplication of a *GS1a* gene in a common ancestor of cycads, ginkgo, and angiosperms (Valderrama-Martín et al., 2022).

GS1b corresponds to the GS1 isoenzyme traditionally studied in model angiosperms. Although this lineage is represented by a unique gene in most of the gymnosperms, in ginkgo and angiosperms, GS1b is represented by a small multigenic family. These genes have different expression patterns depending on the organ and physiological conditions accounting for their different functions (Hirel & Krapp, 2021). These enzymes have been described as key determinants of plant N use efficiency, with essential roles in processes such as senescence (Thomsen et al., 2014), amino acid catabolism, primary assimilation, and different stress responses (Bernard & Habash, 2009). The different genes of this lineage are differentially regulated by developmental state, tissue, nutritional status, and external stimuli (Hirel & Krapp, 2021; Thomsen et al., 2014). Finally, several studies have focused on the enzymatic characterization of GS from angiosperms and gymnosperms (Castro-Rodríguez et al., 2015; de la Torre et al., 2002; Ishiyama et al., 2006; Ishiyama, Inoue, Tabuchi, et al., 2004; Ishiyama, Inoue, Watanabe-Takahashi, et al., 2004; Sakakibara et al., 1996; Yadav, 2009; Zhao et al., 2014) to define a more accurate role landscape for the different GS isoforms.

Some GS1b isoforms are directly related to developmental processes and have been associated with plant productivity. *AtGS1.1* and *AtGS1.2* from *Arabidopsis thaliana* are involved in seed production and germination (Guan et al., 2015). *AtGS1.1* has also been described to be involved in root development during seed germination and *AtGS1.2* plays a role in rosette development (Guan et al., 2015; Lothier et al., 2011). Indeed, a recent study of *AtGS1.1*, *AtGS1.2*, and *AtGS1.3* Arabidopsis mutants suggested synergistic roles for these genes in plant growth and development (Ji et al., 2019). In cereals, enzymes of this GS lineage are involved in seed yield and plant development, such as *GS1;3* from rice (*Oryza sativa*) and barley (*Hordeum vulgare*), which play roles in seed maturation and germination (Fujita et al., 2022; Goodall et al., 2013). *HvGS1.1* overexpression lines showed an improvement in grain yield (Gao et al., 2019). Rice mutants lacking the *OsGS1;1* gene exhibited reduced grain filling and growth (Tabuchi et al., 2005), although the same phenotype was present in rice lines overexpressing *OsGS1;1* (Bao et al., 2014). In addition, rice lines grown in culture chambers and overexpressing *OsGS1;1* presented an increase in spikelet yield. Rice mutants for *OsGS1;2* also presented a depletion in the number of tillers (Funayama et al., 2013), and sorghum (*Sorghum bicolor*) lines overexpressing *GS1* genes exhibited the opposite phenotype (Urriola & Rathore, 2015). Studies in maize (*Zea mays*) using mutant lines for *ZmGS1.3* and *ZmGS1.4* have shown the roles of these genes in kernel number and size, respectively (Martin et al., 2006). Transgenic lines of common bean (*Phaseolus vulgaris*) overexpressing GS1 also showed earlier flower and seed development, while wheat (*Triticum aestivum*) lines overexpressing GS1 showed an increase in grain weight (Habash et al., 2001). Moreover, a recent study on wheat indicated that *TaGS1.1* and *TaGS1.3* are mainly expressed in embryos and grain transport tissues, where these isoforms synergistically carry out ammonium assimilation (Wei et al., 2021).

In conifers, only one isoform of the GS1b family has been identified to date. The unique GS1b identified in conifers has been suggested to play an essential role in N remobilization to developing organs (Suárez et al., 2002). Previous works in pine (*Pinus* spp.) have shown that GS1b is involved in the canalization of ammonium into glutamine during seed germination and the early developmental stages of seedlings (Ávila et al., 2001), which could be important for the loss of seed dormancy (Schneider & Gifford, 1994). Indeed, the roles of GS1b in seed development and germination are also supported by its expression patterns associated with the vascular system of zygotic and somatic pine embryos at different developmental stages and by its expression in procambium cells of pine zygotic embryos (Pérez-Rodríguez et al., 2005). Moreover, the expression of this isoenzyme has been suggested to be controlled by gibberellic acid, a phytohormone involved in many aspects of plant growth and development (Gómez-Maldonado, Cánovas, & Ávila, 2004).

In this work, a gene encoding a cytosolic GS (*PpGS1b.2*) was identified in maritime pine (*Pinus pinaster*). This gene was discovered through sequence searches in transcriptomic data from isolated tissues through laser capture microdissection (Cañas et al., 2017). Orthologs of this gene have also been identified in the genomes of other conifers, and phylogenetic analysis revealed that *PpGS1b.2* belongs to the *GS1b* lineage. Although this *GS1* gene exhibits high sequence homology to the already known *PpGS1b* (hereafter *PpGS1b.1*), *PpGS1b.2* showed low expression levels with characteristic and localized tissue expression. The expression patterns suggest that this gene could play a specific role during plant development, mainly during embryo development, as has been shown for other *GS1b* genes in angiosperms. Furthermore, a detailed comparative analysis of the kinetic properties of the isoenzymes GS1b.1 and GS1b.2 and single/double point mutants of both isoforms support distinct functions for these enzymes in pine.

RESULTS

Sequence and phylogenetic analyses

An unknown cytosolic *GS* gene was identified in a transcriptomic analysis of tissues isolated using laser capture microdissection (Cañas et al., 2017). At the amino acid sequence level, this GS exhibits 80.85% and 92.68% identity with PpGS1a and PpGS1b, respectively (Figure 1a). Despite the high identity between the coding sequences of this gene and *PpGS1b*, the promoter regions of both genes are very distinct (Figure S1). The lengths of the three pine GS proteins are very similar, with 357 residues for PpGS1a, 355 for PpGS1b, and 357 for the enzyme identified in the present study (Figure 1a). However, the calculated isoelectric points were more different between the pine GS proteins, being 6.21 in the case of PpGS1a, 5.73 for PpGS1b, and 5.36 for the protein identified in the present study.

A phylogenetic analysis confirmed the classification of the GSs from seed plants into three main groups, GS2, GS1a, and GS1b, in line with previously reported results (Valderrama-Martín et al., 2022) (Figure 1b). As expected, no GS2 sequence was detected in conifers, but only those of GS1a and GS1b (Figure 1b). The identified GS isoform was grouped within the conifer GS1b sequences; thus, the gene encoding this GS1b isoenzyme has been named *PpGS1b.2*. Orthologs of *PpGS1b.2* have also been detected in other members of the Pinaceae family of the genera *Pinus* and *Picea* but not in the rest of the conifers included in this analysis (Figure 1b).

Gene expression analyses

The expression of *GS* genes in *P. pinaster* has been analyzed in different tissues and conditions to establish a framework that allows us to unravel the potential role of *PpGS1b.2* by comparing its expression pattern to those of other *GS* genes in maritime pine.

The expression profiles were analyzed in embryos and seedlings during the initial developmental stages (Figure 2a). *PpGS1a* expression was high in cotyledons and needles, lower in hypocotyls, and nearly undetectable in roots and embryos except for germinated embryos. *PpGS1b.1* and *PpGS1b.2* expression patterns in embryos were very similar, with a peak of expression in germinated embryos. In seedlings, the expression was ubiquitous in all organs for both genes, although *PpGS1b.2* expression levels were between 5- and 10-fold lower than those of *PpGS1b.1*. This expression pattern was different when isolated tissues were considered (Figure 2b). *PpGS1b.1* was expressed at high levels throughout the plant, especially in the root cortex, where the expression was 40 times that shown by this gene in the other samples. However, *PpGS1b.2* expression was very localized, mainly in the shoot apical meristem, emerging needles, developing root vascularization, and root meristem. Expression was almost undetectable in the rest of the tissues analyzed. Finally, the expression of *PpGS1a* was detected only in the three photosynthetic tissues: the mesophyll of young needles, the mesophyll of cotyledons, and the hypocotyl cortex.

The seasonal expression of the three *GS* genes has also been quantified in needles from adult trees (Figure 3a). *PpGS1a* showed the highest expression, followed by *PpGS1b.1*, whose expression levels were 10 to 30 times lower than those of *PpGS1a*. The expression levels of *PpGS1b.2* were very low compared to those of other *GSs*. The expression patterns of the three genes in different whorls were as before, with higher levels in the first months of the year and lower levels at the end of the year. There was a remarkable exception for whorl 0 in May, the first harvesting month for the needles that emerged during the sampling year. *PpGS1b.2* exhibited an expression peak in whorl 0 in May. In contrast, *PpGS1a* had its lowest expression, and *PpGS1b.1* was expressed at similar levels to the other whorls. The relative abundance of *PpGS1b.2* transcripts was still one and two orders of magnitude lower than those of *PpGS1b.1* and *PpGS1a*, respectively. According to these results, the expression levels of the three genes were also analyzed in buds and emerging needles (Figure 3b–d). The expression of *PpGS1a* was almost undetectable in buds, but its expression rapidly increased in nascent needles by the end of the month. *PpGS1b.1* expression remained almost invariable in both organs with a similar expression pattern. The levels of *PpGS1b.2* were higher in the buds and decreased from day 14 to day 28, when its expression was similar in buds and emerging needles. The relative abundance of *PpGS1b.1* transcripts was still higher than that of *PpGS1b.2*.

GS gene expression has also been analyzed at different developmental stages, including juvenile and mature xylem and phloem, as well as the male and female reproductive structures, different root zones, and different stages of zygotic embryo development (Figure 4). In all those samples, *PpGS1a* expression was barely detectable. An example of *PpGS1a* expression is shown for phloem, xylem, and male and female strobili, with very low levels (<0.04), even in female strobili with an expression peak (<0.08) (Figure 4a). *PpGS1b.1* expression was the highest observed thus far among the *GS* genes analyzed in vascular tissues and strobili (Figure 4a). Interestingly, *PpGS1b.2* expression was almost undetectable in vascular tissues, but its levels peaked in the male strobilus (approximately 0.28), opposite to what occurred with *PpGS1b.1* in that organ. In root samples, *PpGS1b.1* and *PpGS1b.2* presented a similar expression pattern, with increased expression in lateral roots and root tips, although the expression levels for *PpGS1b.1* were approximately 80-fold higher than that shown by *PpGS1b.2* (Figure 4b). Finally, in zygotic embryos, the expression levels of both genes were significantly higher in the pre-cotyledonary and early

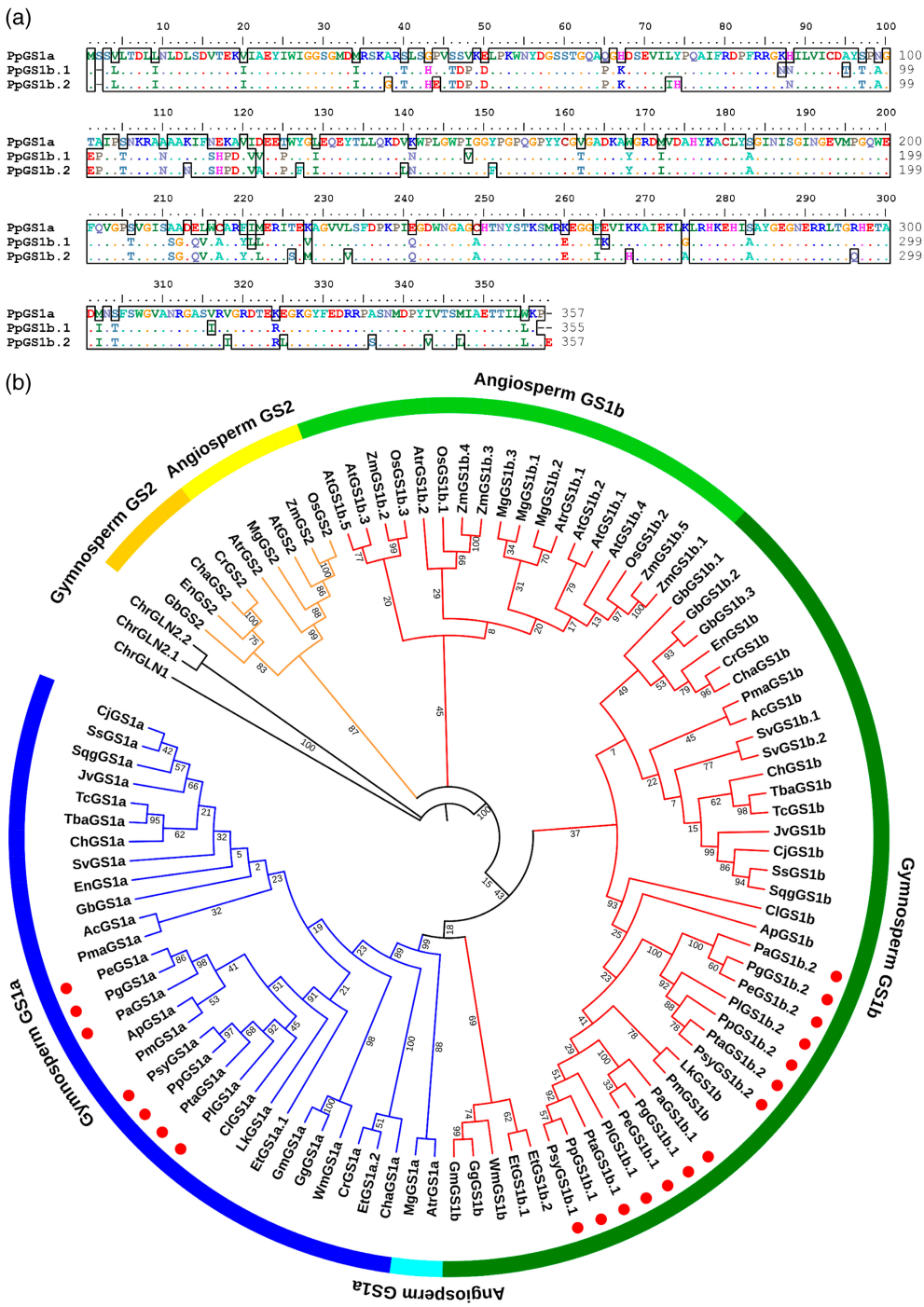

Figure 1. Protein alignment and evolutionary analysis by the maximum-likelihood method. (a) Protein alignment of maritime pine GSs. The PpGS1a sequence is shown as a reference, dots highlight conserved residues in the three sequences. (b) The evolutionary history was inferred by using the maximum-likelihood method and JTT matrix-based model (Jones et al., 1992). The tree with the highest log likelihood (−11 590.51) is shown. The percentage of trees in which the associated taxa clustered together is shown next to the branches. Initial tree(s) for the heuristic search were obtained automatically by applying NJ and BioNJ algorithms to a matrix of pairwise distances estimated using the JTT model and then selecting the topology with superior log likelihood value. The tree is drawn to scale, with branch lengths measured in the number of substitutions per site. This analysis involved 102 amino acid sequences. All positions containing gaps and missing data were eliminated (complete deletion option). There was a total of 348 positions in the final dataset. Evolutionary analyses were conducted in MEGA11 (Tamura et al., 2021). Numbers close to the branches show bootstrap values. The first two letters of the sequence names correspond to the genera and species listed in Table S1. Golden tree branches correspond to GS2 sequences, blue branches to GS1a sequences, and red branches to GS1b sequences. Discontinuous lines in GS1b branches highlight the new sequences found in *Pinus* and *Picea*. Red dots show the sequences from *Pinus* and *Picea*.

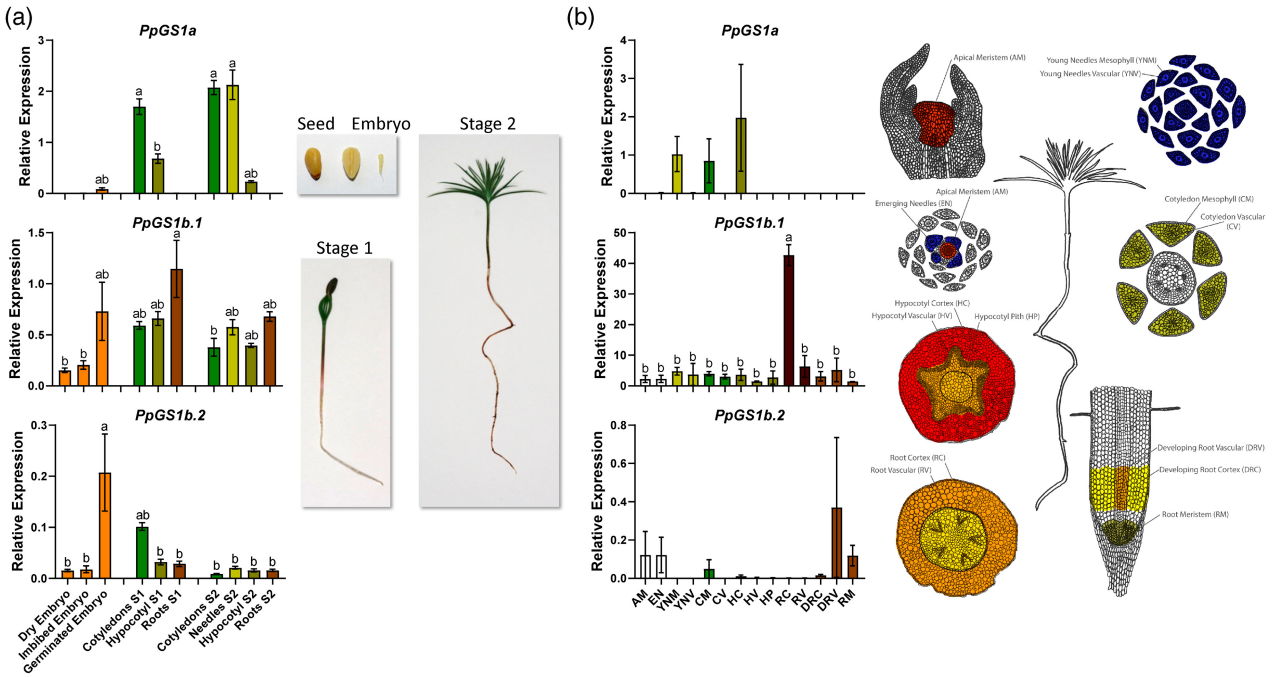

Figure 2. *GS* gene expression in maritime pine seedlings. (a) Expression levels of *GS* genes of maritime pine during germination and initial seedling development. Stage 1 (S1) corresponds to seedlings with active mobilization of reserves from the megagametophyte to the seedling (1 week after emergence). Stage 2 (S2) corresponds to seedlings without megagametophyte and developing the first new needles (1 month after emergence). (b) Gene expression levels of GSs in tissues from 1-month-old seedlings (Cañas et al., 2017). AM, shoot apical meristem; EN, emerging needles; YNM, young needle mesophyll tissue; YNV, young needle vascular tissue; CM, cotyledon mesophyll tissue; CV, cotyledon vascular tissue; HC, hypocotyl cortex; HV, hypocotyl vascular tissue; HP, hypocotyl pith; RC, root cortex; RV, root vascular tissue; DRC, developing root cortex; DRV, developing root vascular tissue; RM, root apical meristem. Different letters above the columns indicate a statistically significant difference ($P < 0.05$) as determined by the Tukey *post hoc* test after analysis of variance. Error bars show SE with $n = 3$.

cotyledonary stages, where *PpGS1b.2* levels were higher than those shown by *PpGS1b.1* (Figure 4c). However, this ratio of the expression of both genes was reversed in the later stages of development in cotyledonary and mature embryos. Nevertheless, the differences in expression between the two genes were not statistically significant in either case.

Protein structure prediction and physicochemical and kinetic properties

Very few differences were observed between the GS1b.1 and GS1b.2 subunit structures due to the similarity of their amino acid sequences (Figure 5a,b). Both proteins presented a predicted decameric structure formed by two pentameric rings with small differences in structure and the disposition of the subunits in the quaternary structure (Figure S2). However, the thermodynamic stability of GS1b.1 monomers was three times higher than that of GS1b.2 monomers (Table 1). The *in silico* replacement of residues of the GS1b.1 and GS1b.2 amino acid sequences displayed some differences in their effects on the structural stability of both enzymes (Figure S3). Some of the amino acids used for this analysis did not cause any notable effects on the structure or destabilized both proteins equally. However, several amino acids gave rise to large differences in the free energy of folding. Specifically, the inclusion of arginine or glutamate around position 280 produced a great destabilization of the structure of GS1b.2 but not of GS1b.1. Some of these amino acids also caused great destabilization of GS1b.2 when substituted at position 148 but did not have the same effect in GS1b.1. In fact, only isoleucine and arginine produced marked effects on the structural stability of GS1b.1. As small differences in the structure suggested that there might be changes in the physicochemical and kinetic properties of both enzymes, a functional comparison of the recombinant isoforms of GS1b.1 and GS1b.2 was performed (Figure 5; Tables 1, 2; Figure S4).

Both isoforms were tested over a wide pH range; GS1b.1 maximum activity was reached at pH 6.5 while GS1b.2 maximum activity was reached at pH 6 (Figure 5c). The activity of both enzymes increased with the reaction temperature, reaching maximum activity at 42°C (Figure 5d). These data allowed the calculation of the activation energy (Ea) for each enzyme (Table 1). The Ea values were different for both enzymes: the Ea value of GS1b.1 was 39.9 kJ mol^{-1}, and the Ea values of GS1b.2 for its elemental reaction steps were 46.1 kJ mol^{-1} and 18.7 kJ

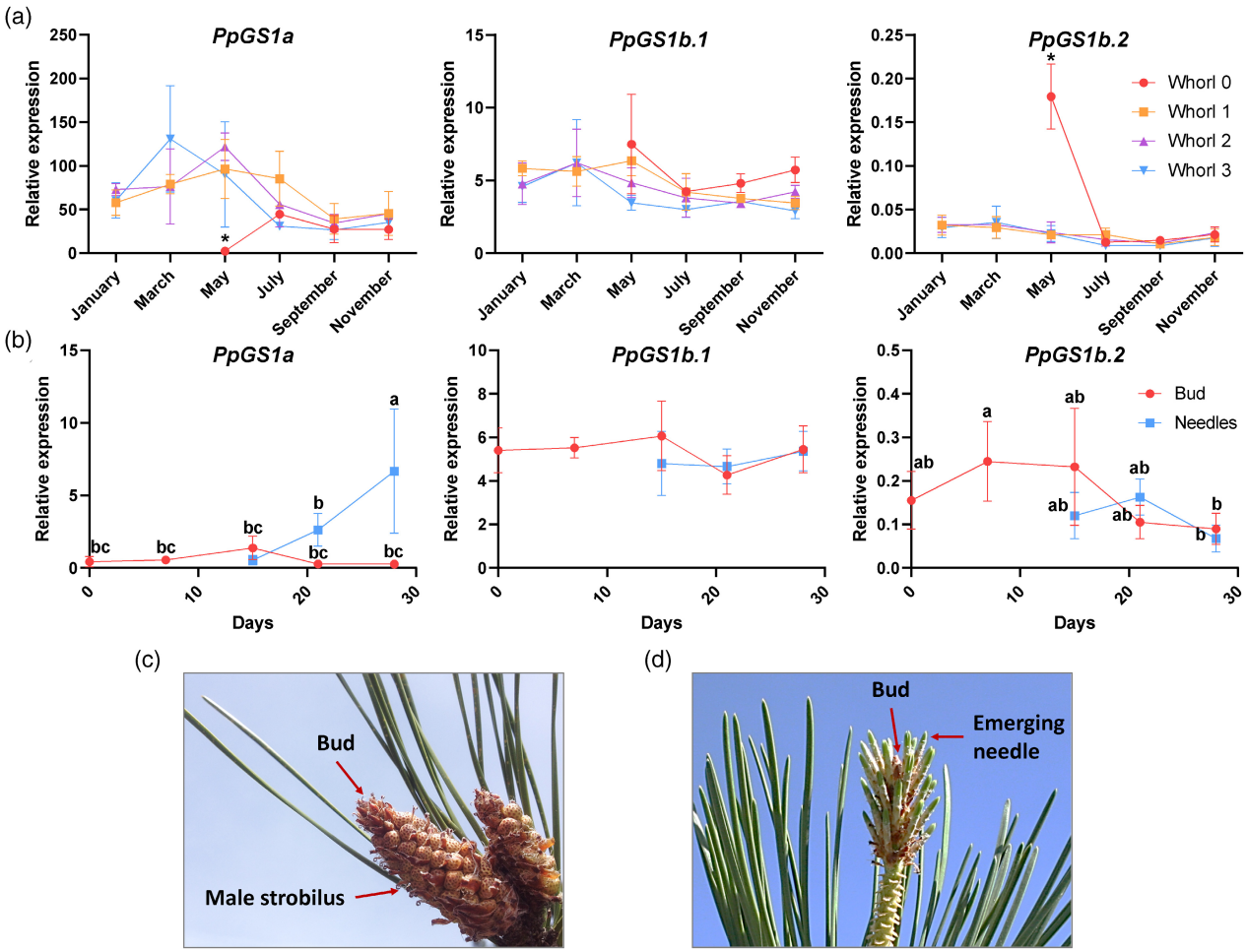

Figure 3. Seasonal *GS* gene expression profiles in pine needles from adult trees. (a) Expression levels of *GS* genes were determined in needles from maritime pine for a year. Each needle whorl corresponds to the annual growth of a single year; the whorls were numbered from 0 to 3, with 3 indicating the oldest whorl. Whorl 0 corresponds to needles that emerged in the year of harvesting. For supplementary information see Cañas et al. (2015). Asterisks above the data points highlight a statistically significant difference ($P < 0.05$) between needle whorls in a specific month as determined by a Tukey *post hoc* test after analysis of variance. Error bars show SE with $n = 3$. (b) Expression levels of *GS* genes in buds and developing needles during the first 21 days of emergence. Different letters above the data points indicate a statistically significant difference ($P < 0.05$) as determined by a Tukey *post hoc* test after analysis of variance. Error bars show SE with $n = 3$. (c) Picture of buds and male strobilus in April during the first harvest. (d) Picture of buds and emerging needles in May at the fourth harvest (21 days).

mol^{-1}, with a break point at 24°C. Regarding thermal stability, GS1b.1 was very stable, only decreasing its activity at 60°C after 5 min of pre-incubation, although it never completely lost its activity, even after 20 min at 60°C (Figure 5e). However, GS1b.2 showed decreased activity even after 5 min of pre-incubation at 45°C, with an almost total loss of activity after 5 min at 60°C (Figure 5e).

GS1b.1 and GS1b.2 showed distinctive behaviors for ammonium and glutamate (Figure 5f,g). GS1b.2 exhibited substrate inhibition for ammonium (K_i, 22.57 mM). The affinities of both enzymes for ammonium were high (GS1b.1 K_m, 0.12 mM; GS1b.2 K_m, 0.21 mM). However, V_{max} was 5.88 times higher for GS1b.1 (Table 2). Regarding glutamate, GS1b.1 showed substrate inhibition at high concentrations (K_i, 84.51 mM), while GS1b.2 presented positive cooperativity. In both cases, the affinity was very low (GS1b.1 K_m, 64.15 mM; GS1b.2 EC_{50}, 48.63 mM), with large differences in the V_{max} values of both enzymes (GS1b.1, 101.6 nkat per mg protein; GS1b.2, 7.66 nkat per mg protein) (Table 2). GS1b.1 and GS1b.2 showed equal behavior for Mg_2^+, with positive cooperativity and similar affinity (EC_{50} values of 14.49 and 10.87 mM, respectively) but different V_{max} values (71.32 and 5.64 nkat per mg protein, respectively) (Figure S4, Table 2). Finally, the affinities for ATP were high and similar for both enzymes (K_m of 0.18 and 0.29 mM for GS1b.1 and GS1b.2, respectively), with a higher V_{max} for GS1b.1 (24.96 nkat per mg protein) than for GS1b.2 (7.39 nkat per mg protein). However, substrate inhibition was observed for GS1b.1 at moderate ATP levels (K_i, 5.88 mM).

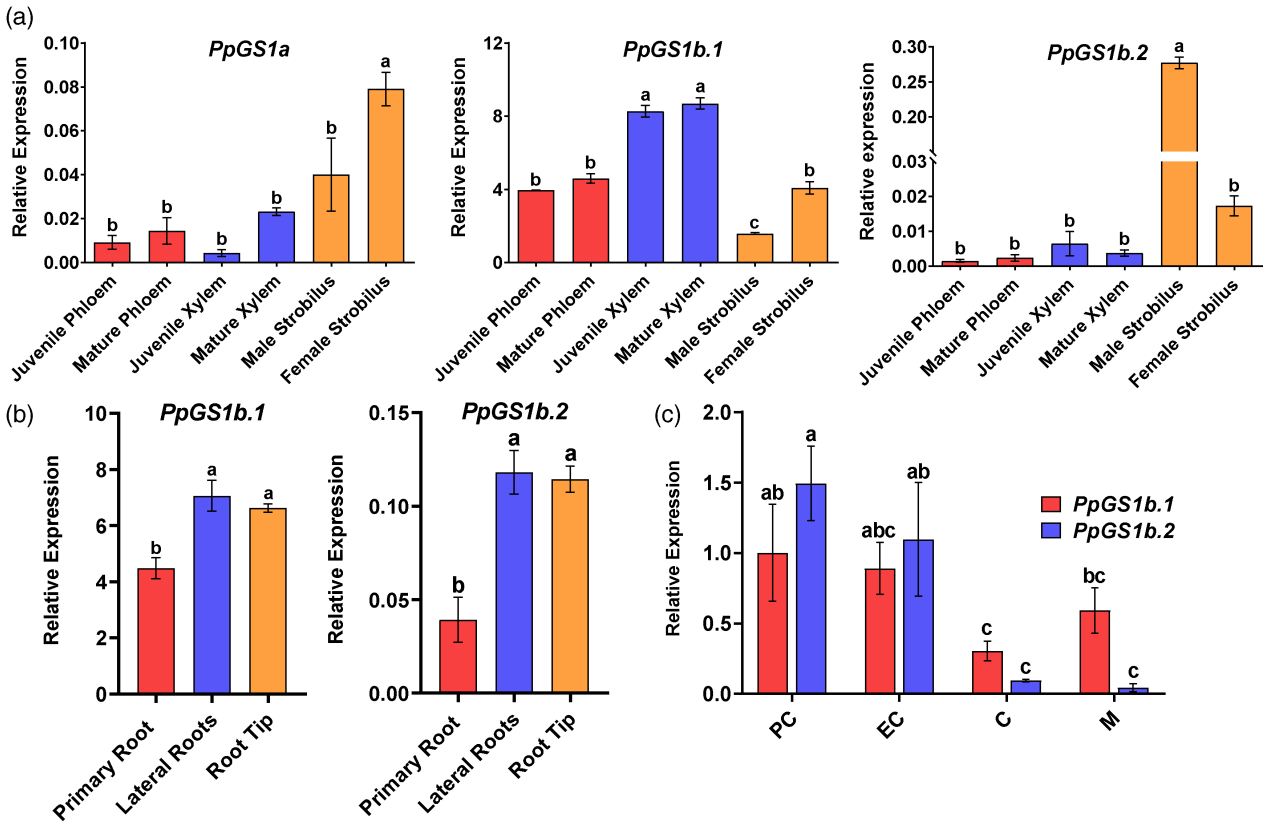

Figure 4. *GS* expression levels in different developing tissues. (a) Gene expression levels of *PpGS1a*, *PpGS1b.1*, and *PpGS1b.2* in different tissues of adult trees: juvenile and mature phloem; juvenile and mature xylem; and male and female strobili. (b) Gene expression of *PpGS1b.1* and *PpGS1b.2* in different parts of the root from 1-month-old seedlings: primary root, lateral roots, and root tip. (c) Gene expression of *PpGS1b.1* and *PpGS1b.2* in different developmental stages of zygotic embryos. PC, pre-cotyledonary stage; EC, early cotyledonary stage; C, cotyledonary stage; M, mature embryo. Different letters above the columns indicate a statistically significant difference ($P < 0.05$) as determined by a Tukey *post hoc* test after analysis of variance. Error bars show SE with $n = 3$.

Analysis of mutant proteins

To determine the roles that certain residues could play in GS activity, GS1b.1 and GS1b.2 mutants were obtained by exchanging amino acids at positions 264 and 267. These residues belong to a region that accumulates a significant number of differences between the two isoforms and is important for stability, as shown by the *in silico* substitution analysis (Figure S3). Additionally, these residues have been selected based on their charge and structural differences between both GSs. The amino acid swapping at positions 264 and 267 seemed to produce only slight changes in subunit arrangement, even in the double mutant. Calculation of hydrogen bonds revealed interactions of residues 264 and 267 with residues 261, 263, 265, and 268. These residues were analyzed in detail, and only small differences in their arrangements could be observed (Figure 6a–g; Figure S5). The quaternary structures of the mutants also showed no significant differences (Figure S6), and the thermodynamic stability of the monomers was similar to that of the wild type (WT) (Table 1).

Compared to WT, none of the optimal pH values were affected in any of the mutants tested, except for GS1b.2 E264K, where the optimum was reached at pH 7 (Figure S7), and the double mutants, where the optimum pH was 6 for both enzymes (Figure 6h; Figure S7).

A slight increase in the optimal temperature (45°C) was detected in all mutants except for GS1b.2 E264K, which experienced a large change in its optimal temperature (30°C) (Figure 6i; Figure S7). Although the activity patterns in response to reaction temperature were similar in the mutants with respect to the WT enzymes, the activity was slightly higher at all temperatures in the GS1b.1 K267H single and GS1b.2 double mutants. In the case of GS1b.1 K264E and GS1b.2 H267K, the activity was higher at temperatures above the optimum (45°C). Finally, the GS1b.1 double mutant retains considerable activity levels (>40%) even at very low reaction temperatures, such as 4°C (Figure 6i; Figure S7). Ea was barely affected (Table 1) in GS1b.1 K264E (34.8 kJ mol^{-1}). In contrast, the Ea value of the GS1b.1 double mutant was strongly affected (15.2 kJ mol^{-1}), and GS1b.1 K267H showed different Ea values for its elemental reaction steps (35.2 kJ mol^{-1} and 6.7 kJ mol^{-1}), similar to GS1b.2 WT. However, GS1b.2 E264K presented a unique Ea for its reaction (39.9 kJ mol^{-1}),

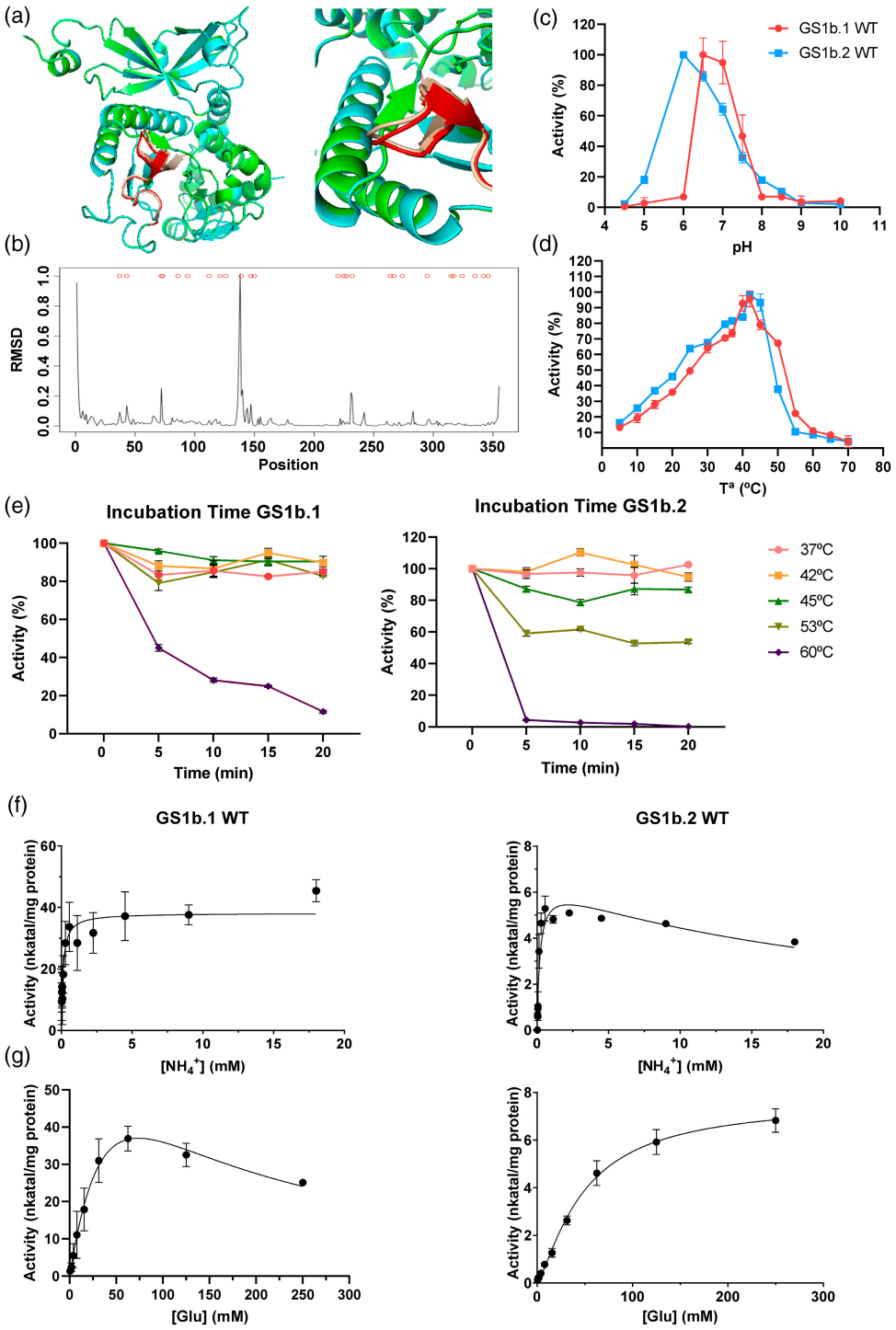

Figure 5. Enzymatic characterization of recombinant GS1b.1 and GS1b.2 isoforms. (a) Comparison of GS1b.1 and GS1b.2 subunit structures. GS1b.1 is represented in green and GS1b.2 in cyan. The region that presented most differences between GS1b.1 and GS1b.2 (amino acids 125 to 150) are represented in red and pink, respectively. (b) Root mean square deviation (RMSD) values between GS1b.1 and GS1b.2 monomer structures. (c) Enzyme activity at different assay pH values (from 4.5 to 10) for GS1b.1 (red line) and GS1b.2 (blue line). (d) Enzyme activity at different assay temperatures (from 5°C to 70°C) for GS1b.1 (red line) and GS1b.2 (blue line). (e) Thermal stability of GS1b.1 and GS1b.2 at different temperatures (37°C, 42°C, 45°C, 53°C, and 60°C) after different pre-incubation times (from 0 to 20 min). (f) Kinetics of GS1b.1 and GS1b.2 for ammonium. (g) Kinetics of GS1b.1 and GS1b.2 for glutamate. Error bars show the SD. Experiments were conducted in at least three independent replicates.

Table 1 Physicochemical properties of WT PpGS1b.1 and PpGS1b.2 and their mutated versions

Property	GS1b.1 WT	GS1b.2 WT	GS1b.1 K264E	GS1b.2 E264K	GS1b.1 K267H	GS1b.2 H267K	GS1b.1 K264E, K267H	GS1b.2 E264K, H267K
Optimum temperature	42	42	45	30	45	45	45	45
Optimum pH	6.5	6	6.5	7	6.5	6	6	6
Monomer ΔG folding (kcal mol^{-1})	−9.7	−2.7	−10.1	−2.3	−9.2	−2.7	−10.0	−2.3
Ea (kJ mol^{-1})	39.8	46.1/18.7	34.8	39.9	35.2 / 6.7	33.7 / 10.3	15.2	28.4 / 6.7
$\Delta G^{\ddagger}$ (kJ/mol)	63.6	62.6 / 62.8	63.5	62.3	62.9 / 62.2	63.1 / 62.4	62.7	62.1 / 62.0
$\Delta H^{\ddagger}$ (kJ mol^{-1})	36.9	43.6 / 16.1	32.3	37.4	32.7 / 4.3	31.2 / 7.9	12.7	25.9 / 4.2
$T\Delta S^{\ddagger}$ (kJ mol^{-1})	−26.7	−19.0 / −46.7	−31.2	−24.9	−30.2 / −57.9	−31.9 / −54.5	−50.0	−36.2 / −57.8
Break (°C)		24			34	35		27.5

Table 2 Kinetic properties of WT PpGS1b.1 and PpGS1b.2 and their mutated versions

Substrate	GS1b.1 WT	GS1b.2 WT	GS1b.1 K264E	GS1b.2 E264K	GS1b.1 K267H	GS1b.2 H267K	GS1b.1 K264E, K267H	GS1b.2 E264K,H267K
NH_4^+	V_{max} 38.15 K_m 0.12	V_{max} 6.48 K_m 0.21 K_i 22.57	V_{max} 21.01 K_m 0.16	V_{max} 16.36 K_m 0.16	V_{max} 79.3 K_m 0.06 K_i 13.14	V_{max} 58.26 K_m 0.05	V_{max} 36.05 K_m 0.02	V_{max} 56.88 K_m 0.09
Glu	V_{max} 101.6 K_m 64.18 K_i 84.51	V_{max} 7.66 nH 1.311 EC_{50} 48.63	V_{max} 16.82 K_m 2.20	V_{max} 15.69 K_m 18.41	Non-saturated	Non-saturated	Non-saturated	Non-saturated
Mg^{2+}	V_{max} 71.32 nH 1.66 EC_{50} 14.49	V_{max} 5.64 nH 2.33 EC_{50} 10.87	Non-saturated	V_{max} 25.43 nH 1.61 EC_{50} 26.78	Non-saturated	Non-saturated	Non-saturated	Non-saturated
ATP	V_{max} 24.96 K_m 0.18 K_i 5.88	V_{max} 7.39 K_m 0.29	V_{max} 29.73 K_m 0.11 K_i 3.19	V_{max} 27.40 K_m 0.21 K_i 8.23	V_{max} 59.82 K_m 0.06 K_i 5.85	V_{max} 28.57 K_m 0.39 K_i 8.76	V_{max} 38.69 K_m 0.09	V_{max} 100.6 K_m 0.42 K_i 5.06

EC_{50} in mM; K_i in mM; K_m in mM; nH is dimensionless; V_{max} in nkat per mg protein. EC_{50}, the concentration of substrate that produces a half-maximal reaction rate; K_i, dissociation constant for substrate binding; K_m, Michaelis–Menten constant; nH, Hill slope; V_{max}, maximal reaction rate.

and different Ea values were detected for the elemental reaction steps of GS1b.2 H267K (33.7 kJ mol^{-1} and 10.3 kJ mol^{-1}) and the GS1b.2 double mutant (28.4 kJ mol^{-1} and 6.7 kJ mol^{-1}). Interestingly, all GS1b.1 mutants experienced decreases in their thermostability compared to the WT, and only GS1b.2 H267K showed an increased thermostability compared to GS1b.2 WT (Figure 6j; Figure S7).

GS1b.1 behavior regarding ammonium was only modified in the GS1b.1 K267H mutant, which showed substrate inhibition for ammonium (K_i, 13.14 mM). Furthermore, the affinity was increased in this mutant, GS1b.2 H267K, and both double mutants (K_m between 0.02 and 0.09 mM). Meanwhile, all GS1b.2 mutants lost their substrate inhibition ability by ammonium, and all exhibited normal hyperbolic saturation (Figure 6k; Table 2; Figure S8). Regarding glutamate, GS1b.1 K264E lost its substrate inhibition ability, now presenting normal hyperbolic saturation with an increase in its affinity (K_m, 2.2 mM) accompanied by a reduction in V_{max} (16.82 nkat per mg protein). Additionally, none of the mutants at residue 267 and double mutants reached saturation and seemed to have lost affinity for this substrate, as occurred with Mg_2^+ in all the mutants except for GS1b.2 E264K (Figures S9 and S10; Table 2). GS1b.1 mutants exhibited substrate inhibition by ATP, but only the double mutants of GS1b.1 lost its substrate inhibition ability by ATP and presented normal hyperbolic saturation for this substrate (Figure S11, Table 2). Interestingly, all GS1b.2 mutants exhibited inhibition by ATP (K_i ranging from 5.06 to 8.76 mM), in contrast to the hyperbolic Michaelis–Menten saturation exhibited by the WT (Figure S11; Table 2).

DISCUSSION

The phylogenetic analysis carried out in this work (Figure 1) grouped the identified GS isoform (GS1b.2) within the

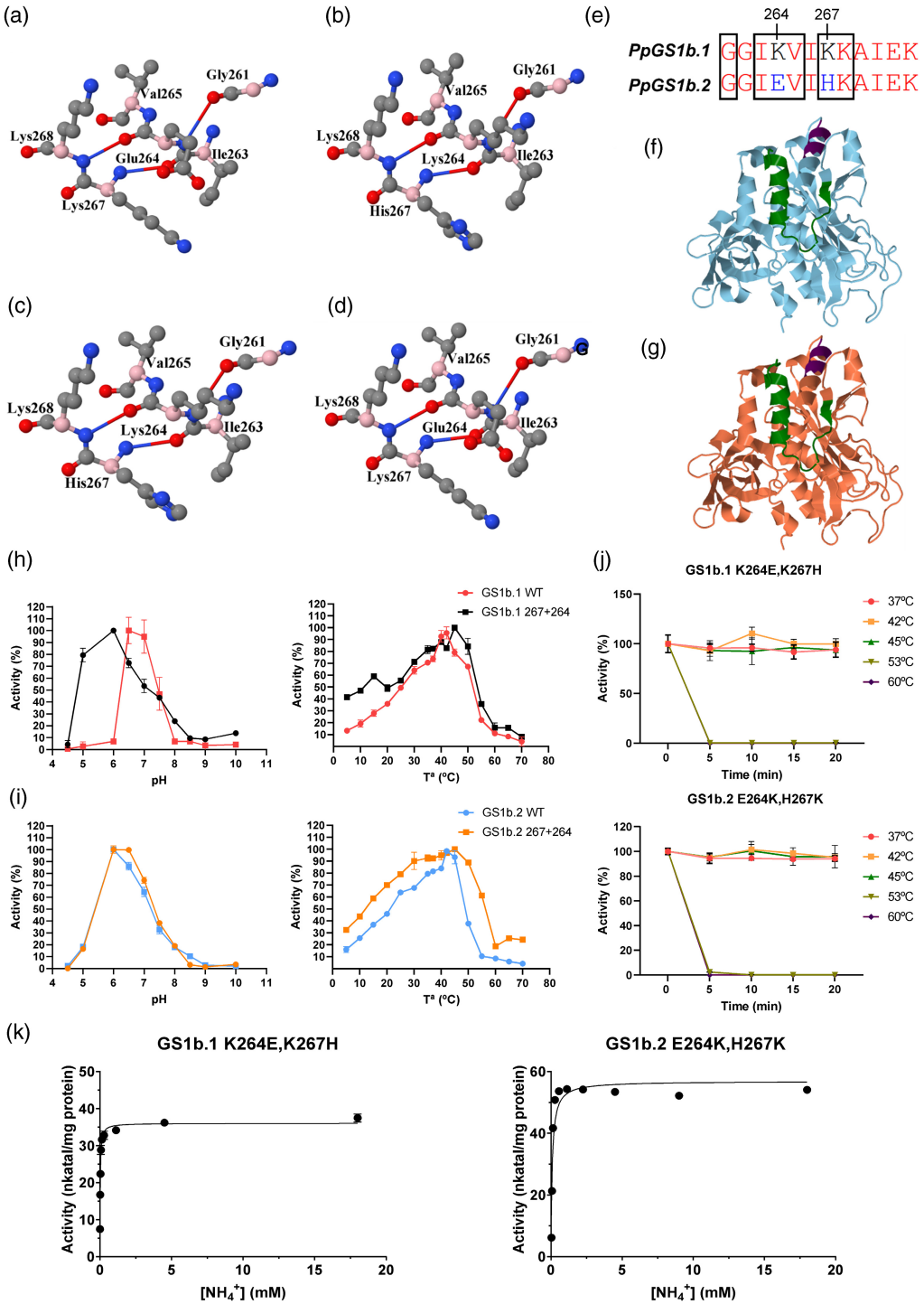

Figure 6. Characterization of mutated GS1b.1 and GS1b.2 proteins. (a–d) Disposition of the amino acids, those that have been exchanged and those associated with them by hydrogen bonds in GS1b.1 K264E (a), GS1b.2 E264K (b), GS1b.1 K267H (c), and GS1b.2 H267K (d) mutants. Alpha carbons of the amino acids are represented in pink. (e) Amino acid region affected by mutations. (f, g) Subunit structures of the GS1b.1 (f) and GS1b.2 (g) double mutant. Amino acids exchanged and amino acids associated with them by hydrogen bonds are represented in dark magenta. Amino acids from residue 330 to the C-terminus of the protein are represented in green. (h) Comparison of the physicochemical properties of GS1b.1 WT and its double mutant. (i) Comparison of the physicochemical properties of GS1b.2 WT and its double mutant. (j) Thermal stability of the double mutants at different temperatures (37°C, 42°C, 45°C, 53°C, and 60°C) after different pre-incubation times (from 0 to 20 min). (k) Kinetics of GS1b.1 and GS1b.2 double mutants for ammonium. Error bars show the SD. Experiments were conducted in at least three independent replicates.

conifer GS1b.1 group. Furthermore, the identification of *GS1b.2* in the genome, its different promoter sequences, including different transcription factor binding sites (Figure S1), and its different gene expression patterns rule out the possibility that it is an allelic variant of *PpGS1b.1* (HF548531.1), suggesting that *PpGS1b.2* (KU641799.1; KU641800.1) is likely the result of a gene duplication. The presence of *GS1b.2* in members of the genera *Pinus* and *Picea* indicates (Figure 1) that this gene duplication should have taken place in a common ancestor of these two groups but not of the entire Pinaceae family, since orthologs of *GS1b.2* have not been identified in other conifers. Gene duplication is very common in plants (De Smet & Van de Peer, 2012), and it could lead to the acquisition of new functions (neofunctionalization) or simply to redundant activity to maintain the correct metabolic flux, as occurred with GS in poplar (*Populus* spp.) and rice (Castro-Rodríguez et al., 2015; Yamaya & Kusano, 2014), contributing to metabolic homeostasis (Moreira et al., 2022). In fact, the GS1b family in angiosperms has been extended by gene duplication so that different isoenzymes can play non-redundant or synergistic roles within the plant, as proposed for *Arabidopsis GS1* genes (Ji et al., 2019).

To explore the possible neofunctionalization of this *GS* isoform after gene duplication, the expression patterns of the maritime pine *GS* genes were analyzed in different organs and tissues (Figures 2–4). *PpGS1b.2* appears to be expressed primarily in developing organs and tissues and is tightly regulated throughout embryonic development. This contrasts with *PpGS1b.1* expression, which was high in all analyzed samples. This could indicate a strong regulation of *PpGS1b.2* at both the localization and expression levels, suggesting a specialized function. The expression of *PpGS1b.2* is consistent with the association of some *GS1b* isogenes with plant developmental processes in angiosperms (Bao et al., 2014; Fujita et al., 2022; Funayama et al., 2013; Gao et al., 2019; Goodall et al., 2013; Guan et al., 2015; Habash et al., 2001; Ji et al., 2019; Lothier et al., 2011; Martin et al., 2006; Tabuchi et al., 2005; Urriola & Rathore, 2015; Wei et al., 2021). These data suggest an evolutionary convergence that has led to the emergence of GS1b isoforms with similar roles in different plant species. The expansion of the GS1b family in certain conifers supports the idea that GS1b diversification in angiosperms responds to different plant needs associated with N assimilation (Hirel & Krapp, 2021). In pine, *GS1b.1* has also been associated with this function due to its expression during zygotic and somatic embryo development (Pérez-Rodríguez et al., 2005). Based on all these expression data, we pose different hypotheses about the role of this isoenzyme: (a) GS1b.2 could support GS1b.1 activity in developing tissues with a high demand for glutamine or assimilated N; and (b) GS1b.2 could play a specific role in certain developing tissues. In this sense, GS1b.2 could play a role similar to that of certain angiosperm GSs that have been described as being involved in developmental processes. In this respect, the enzymatic characteristics of PpGS1b.2 could be more accurate to the needs of developing tissues than those of PpGS1b.1, an enzyme clearly related to global ammonium (N) assimilation in the plant. This could provide an evolutionary advantage.

To explore the differential roles of GS1b.1 and GS1b.2 in maritime pine, the structures and the physicochemical and kinetic properties of both enzymes were analyzed. Modeling of both maritime pine GS1b isoforms revealed small differences between GS1b.1 and GS1b.2 when their tertiary and quaternary structures were compared (Figure 5a,b; Figure S2). However, any minor difference in subunit arrangements could be of great importance since the GS active site is formed by the N- and C-terminal domains of adjacent subunits (Llorca et al., 2006).

Although GS1b.1 and GS1b.2 are very similar in their primary sequences and structures, quite a few differences have been found in their properties. The thermodynamic stability of GS1b.1 was three times higher than that of GS1b.2 (Table 1). Both isoenzymes present similar values (approximately 63 kJ mol^{-1}) for the change in Gibbs free activation energy ($\Delta G^{\ddagger}$), but their kinetic response to temperature changes below and above 24°C may be very different (Table 1). For GS1b.2, $\Delta G^{\ddagger}$ and the rate-limiting step are dominated by different activation parameters at different operating temperatures: $\Delta H^{\ddagger}$ for temperatures below 24°C and $T\Delta S^{\ddagger}$ for temperatures above 24°C. In contrast, GS1b.1 showed non-variable activation energy throughout the whole range of temperatures assayed (Table 1). These differences in dominant activation parameters could reflect functional differences between the two active sites, as has been previously suggested for GS isoforms from other sources (Wedler & Horn, 1976).

The optimum pH levels for GS1b.1 and GS1b.2 are 6.5 and 6, respectively (Table 1; Figure 5c), similar to those of GS1b.2 and GS1b.3 from poplar (Castro-Rodríguez et al., 2015). Interestingly, these optimal pH values are lower than the cytosolic pH (7.1–7.5) (Zhou et al., 2021), which could be a mechanism to avoid enzyme inhibition by the acidification process associated with GS activity and ammonium (Hachiya et al., 2021). The optimum temperature for both enzymes (42°C) (Table 1; Figure 5d) is very similar to that shown by GS1b isoenzymes in other plants (Castro-Rodríguez et al., 2015; Zhao et al., 2014). However, both GS1b enzymes had exceptional thermostability compared to other GS1b enzymes of plants (Figure 5e) (Castro-Rodríguez et al., 2015; Sakakibara et al., 1996; Zhao et al., 2014). Concerning glutamate and ATP, GS1b.1 exhibited substrate inhibition behavior, as previously observed for Arabidopsis GLN1;3 (Table 2; Figure 5g) (Ishiyama, Inoue, Watanabe-Takahashi, et al., 2004). These inhibitions are consistent with the role of GS1b.1 in primary N

assimilation in pine and its high expression since high levels of glutamate and ATP, outside of their homeostatic ranges, could indicate metabolic and energetic problems in the cell that may result in unnecessary or detrimental large-scale N assimilation. Interestingly, GS1b.2 exhibited positive cooperativity for glutamate (Table 2; Figure 5g) and showed substrate inhibition for ammonium (Table 2; Figure 5f). The positive cooperativity mechanism provides high sensitivity to fluctuating substrate concentrations (Levitzki & Koshland Jr, 1976), enabling GS1b.2 to respond rapidly to changes in glutamate availability. In this case, the inhibition of GS1b.2 by ammonium could lead to control of the levels of the final product or to a specific function in the signaling pathway of one of its substrates. This is because both the end product and the substrate of the GS/GOGAT cycle, glutamate and ammonium, have been reported to play roles in plant growth and development (Qiu et al., 2020; Ortigosa *et al.*, 2021), where GS could act as an integrating link for both signaling pathways. Interestingly, glutamate has been described to play important roles in seed germination (Kong et al., 2015), root architecture (Forde, 2014; López-Bucio et al., 2019), and pollen germination and pollen tube growth (Michard et al., 2011; Wudick et al., 2018), among other functions (Qiu et al., 2020). Ammonium has recently been shown to modulate plant root architecture in pine seedlings (Ortigosa et al., 2022). Therefore, based on the *PpGS1b.2* expression patterns, the kinetic characteristics toward glutamate, and previous works, this enzyme could be involved in developmental processes. Furthermore, this could also be a mechanism to avoid high GS activity levels when ammonium is in excess, which could lead to excessive cytosol acidification (Hachiya et al., 2021) of sensitive cells in developing tissues.

The structural, physicochemical, and kinetic analysis carried out in this work on the mutant enzymes showed some differences from the WT isoforms, but almost none of them achieved a complete exchange of the properties between GS1b.1 and GS1b.2. The mutations tested in this work did not greatly affect the protein structure, either in the surroundings of the exchanged amino acids and the subunit structure (Figure 6a–g) or in the quaternary structure (Figure S6), which could explain why the thermodynamic stability of the mutants was not compromised in any case (Table 1). Although all the mutants presented alterations in the activity levels at the different pH values and temperatures analyzed in comparison with the WT, only GS1b.1 K264E,K267H and GS1b.2 E264K produced variations in the optimal pH, and only GS1b.2 E264K presented a considerable variation in its optimum temperature (Figure S7) and Ea (Table 1). In fact, among all the mutants, GS1b.2 E264K presented the greatest number of changes in physicochemical properties. In fact, this could indicate that none of these amino acids are highly involved in these enzyme properties or, perhaps, that the changes that can produce these mutations are being buffered by other residues.

Interestingly, these mutations had large effects on the kinetic properties (Table 2; Figure 6k; Figures S8–S11). The results suggest that these residues are involved in affinity toward ammonium. Although it has been described that the presence of glutamine and serine at positions 49 and 174, respectively, is essential for the high affinity for ammonium in Arabidopsis GS (Ishiyama et al., 2006), these residues are not present in either GS1b.1 or GS1b.2 of *P. pinaster*. Previous kinetic studies have shown the presence of high-affinity GS isoforms that either do not have this combination of amino acids or have none of them (Castro-Rodríguez et al., 2015; de la Torre et al., 2002; Sakakibara et al., 1996; Yadav, 2009; Zhao et al., 2014). These previous works and the current results support the hypothesis proposed by Castro-Rodríguez et al. (2015), indicating that key residues determining GS behavior for ammonium may vary between plant species.

Mutations have produced a great number of changes in the behavior of these enzymes towards their substrates and in their kinetic parameters. However, a reversal has only been achieved for ATP in double mutants, suggesting that the differences in these properties are due to the collaborative efforts of several residues, probably those that differ between the two enzymes. This may indicate that GS1b.1 and GS1b.2 have undergone evolutionary selection so that the two enzymes satisfy different plant needs, with only minor changes in their amino acid sequences. This hypothesis is also supported by the differences between the two enzymes at the structural stability level (Figure S3). When introduced at certain positions, some amino acids had a large effect on the protein stability of one isoform but not the other. The region between amino acids 260–300 of GS1b.2 was particularly affected by the introduction of some amino acids, but none of these substitutions appear to produce similar effects in GS1b.1. In fact, these data suggest that the two enzymes are following different evolutionary paths, although further experiments will be required to confirm this hypothesis.

EXPERIMENTAL PROCEDURES

Sequence identification and phylogenetic analyses

The phylogenetic analysis was conducted using protein sequences of plant GSs that were obtained from online public databases or assembled from transcriptomic data contained in the SRA database at the NCBI, except for *P. pinaster* sequences that were cloned and sequenced (Table S1). To obtain the sequences, the procedure presented in Valderrama-Martín et al. (2022) was followed. Briefly, *tblastn* was used in BLAST searches (Altschul et al., 1990) using GS1b.1 from *Pinus taeda* as the query. Transcriptomic assemblies were made using the web platform Galaxy (Afgan et al., 2018). Raw reads were trimmed using *trimmomatic* (Bolger et al., 2014) and assembled with *Trinity* (Grabherr et al., 2011). Database identifiers, names, and species for the

different GS sequences are presented in Table S1. All protein sequences used in the present work are available in Dataset S1.

The sequence dataset was composed of 102 GS proteins. The phylogenetic analysis was mainly focused on conifer GS sequences. Alignment and phylogenetic analysis were conducted as described in Valderrama-Martín et al. (2022) using MEGA version 11 (Tamura et al., 2021). The alignment was conducted with *muscle* (Edgar, 2004). The phylogenetic analysis was carried out through a maximum-likelihood estimation with complete deletion of gaps, the missing data, and the Jones–Taylor–Thornton (JTT) amino acid substitution model (Jones et al., 1992). Nearest-neighbor interchange was used for tree inference. The initial tree was constructed using the NJ/BioNJ method. The phylogeny test was performed using the bootstrap method with 1000 replicates. The GS sequences of *Chlamydomonas reinhardtii* were used as the outgroup. The distance matrix and the original tree in Newick format are available in Datasets S2 and S3. The original tree was visualized with the Interactive Tree of Life web tool (Letunic & Bork, 2019).

Protein structure prediction and modeling

For the 3D modeling and structure predictions of individual *P. pinaster* GS1b.1 and GS1b.2 subunits, AlphaFold (Jumper et al., 2021; Varadi et al., 2022) was used through ColabFold (Mirdita et al., 2022). ColabFold allows faster protein structure prediction by integrating MMseqs2 for multiple sequence alignments and AlphaFold2, but it does not allow the structure prediction of large protein subunits or complexes. Quaternary structure prediction was achieved using AlphaFold's models as input for the Galaxy Package, a combination of several programs that have been designed based on sequence and structure information together with physical chemistry principles (Shin et al., 2014). The models obtained from ColabFold were employed for the comparison and graphic representation of the protein structures in PyMol (https://pymol.org/2/) and in Jmol (http://www.jmol.org/). Jmol was also used for the calculation of the hydrogen bonds. Quaternary structure models obtained with AlphaFold and the Galaxy Package were used in PyMol for the structural analysis and comparison of the models. The thermodynamic stability of the monomers was determined using models obtained in AlphaFold together with the 'foldx.mut()' function of the 'ptm' R package (Aledo, 2021).

Plant material

Maritime pine seeds (*P. pinaster* Aiton) from *Sierra Segura y Alcaraz* (Albacete, Spain) (ES17, Ident. 09/10) were provided by the *Red de Centros Nacionales de Recursos Genéticos Forestales* of the Spanish *Ministerio para la Transición Ecológica y el Reto Demográfico* with authorization number ESNC103. Pine seeds were imbibed for 48 h in water with aeration to induce germination. Seeds were germinated in vermiculite. Seedlings were grown in plant growth chambers (Aralab Fitoclima 1200, Rio de Mouro, Portugal) under a 16 h light photoperiod, with a light intensity of 125 μmol m^{-2} sec^{-1}, a constant temperature of 23°C, and 50% relative humidity, and watered twice a week with distilled water. Embryo and seedling samples were harvested at different stages: dry, post-imbibition, and germinated (0.5 cm of emerged radicle) embryos, 1 week after emergence (Stage 1), and 1 month after emergence (Stage 2). At harvest, seedlings were divided into their different organs. For the measurement of *GS* gene expression in different sections of roots, 2-month-old seedlings were used. The samples were immediately frozen in liquid N_2 and stored at −80°C until pulverization with a mixer mill MM400 (Retsh, Haan, Germany) and further analyses.

Plant material and cDNA to analyze *GS* gene expression levels in maritime pine tissues from 1-month-old seedlings were previously obtained by Cañas et al. (2017). RNA samples from 14 tissues isolated through laser capture microdissection were employed. cDNA was synthesized and amplified as described by Cañas et al. (2014).

Samples from Cañas et al. (2015) were used to analyze *GS* gene expression in needles of adult trees. Briefly, needle whorls corresponding to the annual growth of a single year were harvested from different 25-year-old *P. pinaster* specimens at *Los Reales de Sierra Bermeja* (Estepona, Spain). Whorls were named from 0 to 3 referring to the year of appearance of that whorl. Whorl 0 was first collected in May when it was completely formed. Samples were collected each month throughout 2012, immediately frozen in liquid N_2, and stored at −80°C until their utilization for RNA extraction. Buds and nascent needles were collected from the same adult specimens once a week during April of 2013. For gene expression analyses, three different trees were employed.

Juvenile and mature phloem and male and female strobili were harvested from 25- to 35-year-old maritime pines located at *Los Reales de Sierra Bermeja* (Estepona, Spain). Juvenile xylems were collected from the last five internodes in the crown and mature xylem from the base of the trunk of 28- to 31-year-old maritime pines from *Los Reales de Sierra Bermeja* by removing bark and phloem and scraping with a sterile blade (Villalobos, 2008). All tissues were frozen immediately using liquid N_2 and stored at −80°C until use.

Zygotic embryos from *P. pinaster* were obtained from a single maritime pine seed orchard (PP-VG-014, Picard, Saint-Laurent-Médoc, France) and collected at different developmental stages (Ávila et al., 2022). All samples were frozen in liquid N_2 and stored at −80°C until use.

RNA extraction and RT-qPCR

Total RNA from maritime pine samples was extracted following Canales et al. (2012). RNA concentration and purity (A_{260}/A_{280}) were determined using a NanoDrop© ND-1000 spectrophotometer (ThermoFisher Scientific, Waltham, MA, USA). RNA integrity was checked by electrophoresis. iScript Reverse Transcription Supermix (Bio-Rad, Hercules, CA, USA) was used for the reverse transcription of 500 ng of total RNA of each sample in a total reaction volume of 10 μL, including 2 μL of reaction buffer and 0.5 μL of reverse transcriptase enzyme in a thermal cycler with the following conditions: 30 min at 42°C, 10 min at 65°C, hold at 4°C.

For the reverse transcription-qPCR (RT-qPCR) analysis, three biological samples were used with three technical replicates each. qPCR was carried out using 5 μL SsoFastTM EvaGreen® Supermix (Bio-Rad, Hercules, CA, USA), 10 ng of cDNA, and 20 pmol of each primer in a total reaction volume of 10 μL on a C1000™ Thermal Cycler with a CFX384™ Touch Realm-Time PCR Detection System (Bio-Rad, Hercules, CA, USA) with the following conditions: initial denaturation at 95°C for 2 min, followed by 40 cycles of denaturation at 95°C for 5 sec and elongation at 60°C for 20 sec. Finally, a melt curve was developed from 65°C to 95°C with increments of 0.5°C each 5 sec. Two maritime pine *saposin-like aspartyl protease* and *RNA binding protein* genes were used for normalization (Granados et al., 2016). Expression data were analyzed using the *qpcR* R library and the MAK3 model (Ritz & Spiess, 2008). The primers used for RT-qPCR assays are presented in Table S2.

Cloning, mutagenesis, recombinant expression, and purification of GS1b.1 and GS1b.2

In the search for other *GS* genes in conifers, three genes in *P. pinaster* have been identified in transcriptome databases, named

PpGS1a, *PpGS1b.1*, and *PpGS1b.2*. cDNA of the three genes was amplified by PCR using iProof HF Master Mix (Bio-Rad, Hercules, CA, USA) and cloned into the pJET1.2 vector (ThermoFisher Scientific, Waltham, MA, USA) following the manufacturers' instructions. The used primers were designed from sequences obtained from the maritime pine transcriptome assembled in Cañas et al. (2017). Primers are shown in Table S2. *PpGS1a* was obtained from amplified cDNA of emerging needles (EN) isolated in Cañas et al. (2017). *PpGS1b.1* and *PpGS1b.2* were obtained from amplified cDNA of developing root cortex (DRC) isolated in Cañas et al. (2017).

For recombinant protein expression, the coding sequences of WT *PpGS1b.1* and *PpGS1b.2* were subcloned into the pET30a vector (Merck, Darmstadt, Germany) including an N-terminal 6xHis-tag by PCR. For this task, *Ase*I and *Xho*I sites were added to the *PpGS1b.1* 5′ and 3′ ends, respectively, while *Nde*I and *Xho*I sites were added to the *PpGS1b.2* 5′ and 3′ ends, respectively. These restriction sites along with the 6xHis-tag were introduced by PCR. Primers used are listed in Table S2. The plasmid and PCR product were then cut using the appropriate restriction enzymes and the PCR product was inserted into the plasmid using T4 DNA ligase.

Plasmids were expressed in *Escherichia coli* strain BL-21 (DE3) RIL cells (Agilent, Santa Clara, CA, USA). For protein expression, bacterial clones were grown at 37°C and 180 rpm in an orbital shaker with 500 mL of Luria-Bertani medium supplemented with kanamycin (0.05 mg mL^{-1}) and chloramphenicol (0.034 mg mL^{-1}). When the optical density reached a value of 0.5–0.6 at 600 nm, cultures were tempered and isopropyl-β-D-thiogalactoside was added to a final concentration of 1 mM to induce protein expression. Once the isopropyl-β-D-thiogalactoside was supplied, the cultures were incubated at 25°C and 120 rpm for 5 h, and the cells were collected by centrifugation. The bacterial pellet was resuspended in 5 mL of buffer A (50 mM Tris pH 8, 300 mM NaCl, and 250 mM imidazole) with 4 mg of lysozyme and incubated for 30 min on ice. Then bacteria were lysed by ultrasonication with 20 pulses of 5 sec at 20% amplitude with 5 sec rest between pulses in a Branson Sonifier® Digital SFX 550 (Branson Ultrasonics, CT, USA). The soluble fraction was clarified by centrifugation (1620 ***g*** at 4°C for 30 min). Proteins from the soluble fraction were purified by affinity chromatography with Protino Ni-TED Packed Columns 2000 (Macherey-Nagel, Düren, Germany) based on the His-tag tail. The soluble fraction from bacterial lysate was loaded in a column previously equilibrated with buffer A. Protein elution was performed by adding buffer B (50 mM Tris pH 8, 300 mM NaCl, 250 mM imidazole), and a total of 9 mL of eluate was recovered in 1-mL fractions. Collected fractions were quantified by the Bradford method (Bradford, 1976) and analyzed by SDS-PAGE and Western blot using GS-specific antibodies obtained from rabbit (Figure S12) (Cantón et al., 1996). Fractions containing the proteins were concentrated with Amicon® Ultra-15 Centrifugal Filters Ultracel®-100 K (Merck-Millipore, Burlington, Massachusetts, State of Virginia) with 100-kDa pores and the resulting concentrate was stored in 50% (v/v) glycerol at −20°C for later kinetic measurements and physicochemical analyses.

Site-directed mutagenesis

Considering the characteristics and properties of differing amino acids between GS1b.1 and GS1b.2, residues at positions 264 and 267 were selected for mutagenesis. Site-directed mutagenesis was carried out following Edelheit et al. (2009). The WT coding sequences were amplified from the pET30a vector by PCR using two reverse-complementary primers (Table S2) that already included the mutation to be introduced. The primers were used separately in a PCR reaction using 50 or 500 ng of plasmid and 10 pmol of each primer. The final products of both reactions were then mixed and hybridized. The PCR products were checked on an agarose gel and purified using NucleoSpin® Gel and PCR Clean-up (Macherey-Nagel, Düren, Germany). Finally, the PCR product was digested with FastDigest® *Dpn*I (ThermoFisher Scientific, Waltham, MA, USA) to degrade the vector used as template for the amplification.

Physicochemical assays

Physicochemical properties were determined by conducting the transferase assay as described in Cánovas et al. (1991). Reactions were carried out in 96-well microtiter plates with a final reaction volume of 150 μL. The reaction mixture contained 90.6 mM MOPS pH 7, 20 mM arsenate, 2.93 mM $MnCl_2$, 60 mM NH_2OH, and 0.4 mM ADP. When determining the optimal pH level for the activity of the different isoforms, different buffers were used instead: acetate (4.5–5), MES (6–6.5), HEPES (7–7.5), Tris (8–8.5), and sodium carbonate (9–10). The reaction was initiated by adding glutamine at a final concentration of 120 mM and, after 15 min of incubation at 37°C, 150 μL of STOP solution (10% $FeCl_3 \bullet 6H_2O$ in 0.2 N HCl, 24% trichloroacetic acid, and 5% HCl) was added to stop the reaction. Finally, the plate was centrifuged for 3 min at 3220 ***g***, and 100 μL of the reaction volume was used to measure absorbance at 540 nm in a PowerWave HY (BioTek, Winooski, VT, USA) plate reader. For thermostability characterization, proteins were pre-incubated for different periods and at different temperatures before adding the reaction mix.

Kinetic assays

For the quantification of the kinetic properties, biosynthetic assays were carried out as described by Gawronski and Benson (2004) with some modifications. Reactions were conducted in 96-well microtiter plates in a final volume of 100 μL. GS activity was determined as a function of NADH absorbance depletion at 340 nm in a coupled reaction using lactate dehydrogenase (LDH, EC 1.1.1.27) and pyruvate kinase (PyrK, EC 2.7.1.40). The following reaction mixture was used: 50 mM HEPES pH 7, 10 mM $MgCl_2$, 60 mM NH_4Cl, 250 mM glutamate, 6.25 mM ATP, 1 mM phosphoenolpyruvate, 0.6 mM NADH, 1 U PyrK and 1 U LDH. Reactions were pre-incubated for 5 min at 37°C and GS activity was initiated by adding different concentrations of the substrate that was being analyzed. Reactions were developed for 40 min at 37°C with shaking and absorbance was measured at 340 nm each minute. Analysis of the kinetic characteristics of GS1b.1 WT, GS1b.2 WT, and their mutants were performed with GraphPad Prism 8.0.0 (GraphPad, San Diego, CA, USA).

ACCESSION NUMBERS

The cDNA sequence data have been submitted to the GenBank database under accession numbers KU641797 (PpGS1a); KU641798 and HF548531.1 (PpGS1b.1); and KU641796, KU641799.1, and KU641800.1 (PpGS1b.2).

AUTHOR CONTRIBUTIONS

JMVM, FO, and RAC performed the experiments. RAC performed the phylogenetic analysis. JMVM and JCA performed the *in silico* structural protein analyses. JMVM and RAC wrote the manuscript. FO, JCA, CA, and FMC made additional contributions and edited the manuscript. JMVM and RAC planned and designed the research. RAC, CA, and FMC were responsible for funding acquisition.

ACKNOWLEDGMENTS

The authors are grateful to Professor Francisco Ruiz Cantón for the kind supply of adult tree samples, to Jean François Trontin for the kind supply of embryo samples, and to José Miguel Granados for his help during needle harvesting. This work was funded by the Spanish *Ministerio de Economía y Competitividad*, grant numbers BIO2015-73512-JIN MINECO/AEI/FEDER, UE, and BIO2015-69285-R; and *Ministerio de Ciencia e Innovación*, grant number RTI2018-094041-B-100. This work was also supported by *Junta de Andalucía*, grant number P20_00036 PAIDI 2020/FEDER, UE, and the *Universidad de Málaga*, grant B4-2021-01 (Ayudas Plan Propio). JMVM was supported by a scholarship from the Spanish *Ministerio de Educación y Formación Profesional* (FPU17/03517). FO was supported by a grant from the *Universidad de Málaga* (*Programa Operativo de Empleo Juvenil vía* SNJG, UMAJI11, FEDER, FSE, *Junta de Andalucía*) and funds of the research group BIO-114 (*Biología Molecular y Biotecnología*) from PAIDI, *Junta de Andalucía*. Funding for open access charge: Universidad de Málaga/CBUA.

CONFLICT OF INTEREST

The authors declare that they have no conflicts of interest in relation to the content of this manuscript.

SUPPORTING INFORMATION

Additional Supporting Information may be found in the online version of this article.

Dataset S1. Protein sequences used for phylogenetic analysis.

Dataset S2. Phylogenetic distance matrix.

Dataset S3. Original tree resulting from phylogenetic analysis in Newick format.

Figure S1. Promoter region analysis of *PpGS1b.1* and *PpGS1b.2*. For promoter comparison, 1916 and 2408 nucleotides upstream of the start codons of *PpGS1b.1* and *PpGS1b.2* were recovered from genomic data, respectively (Sterck et al., 2022). (a) Sequence alignment of the promoter regions. Position 1995 corresponds to 1 nt before the start codon. (b) Putative transcription factor binding sites identified using the PlantRegMap prediction tool (Tian et al., 2020).

Figure S2. GS1b.1 WT and GS1b.2 WT quaternary structures. (a) GS1b.1 WT quaternary structure. (b) GS1b.2 WT quaternary structure.

Figure S3. Structural stability of GS1b.1 and GS1b.2 upon amino acid substitutions. The indicated amino acids were substituted in GS1b.1 and GS1b.2. The differences in the folding free energy between WT and mutant (ΔΔG) for GS1b.1 and GS1b.2 are compared (square plots). The rectangular plots represent the difference between GS1b.1 ΔΔG and GS1b.2 ΔΔG (*y*-axis) for each position (*x*-axis).

Figure S4. Representation of kinetic characteristics of GS1b.1 WT and GS1b.2 WT for magnesium and ATP. (a) Magnesium. (b) ATP.

Figure S5. Subunit structure of the GS1b.1 and GS1b.2 mutants. (a) GS1b.1 K264E. (b) GS1b.1 K267H. (c) GS1b.2 E264K. (d) GS1b.2 H267K. Amino acids exchanged and amino acids associated with them by hydrogen bonds are represented in dark magenta. Amino acids from 330 to the end of the protein are represented in green.

Figure S6. Quaternary structure of the GS1b.1 and GS1b.2 mutants. (a) GS1b.1 K264E. (b) GS1b.1 K267H. (c) GS1b.1 K264E, K267H. (d) GS1b.2 E264K. (e) GS1b.2 H267K. (f) GS1b.2 E264K, H267K.

Figure S7. Physicochemical properties of the GS1b.1 and GS1b.2 mutants. Activities of GS1b.1 K264E, GS1b.1 K267H, GS1b.2 E264K, and GS1b.2 H267K were tested at different pH levels (a) and temperatures (b). Their thermal stability has been also characterized (c).

Figure S8. Representation of kinetic characteristics of GS1b.1 and GS1b.2 single mutants for ammonium.

Figure S9. Representation of kinetic characteristics of GS1b.1 and GS1b.2 single and double mutants for glutamate.

Figure S10. Representation of kinetic characteristics of GS1b.1 and GS1b.2 single and double mutants for magnesium.

Figure S11. Representation of kinetic characteristics of GS1b.1 and GS1b.2 mutants for ATP.

Figure S12. Purification of recombinant GS proteins. (a) Coomassie staining of SDS-PAGE gels. (b) Western blot analysis using GS-specific antibodies for GS1b.1 and GS1b.2 detection. Molecular weight ladder (L), soluble fraction (S), binding fraction (B), wash step 1 (W1), wash step 2 (W2), elution 1 to 9 (E1–9), and concentrated fraction (C).

Table S1. GSs used for phylogenetic analysis.

Table S2. List of primers.

OPEN RESEARCH BADGES

This article has earned an Open Data badge for making publicly available the digitally-shareable data necessary to reproduce the reported results. The data is available at [PpGS1a cDNA https://www.ncbi.nlm.nih.gov/nuccore/KU641797.1/; PpGS1b.1 cDNA https://www.ncbi.nlm.nih.gov/nuccore/KU641798; PpGS1b.1 gene https://www.ncbi.nlm.nih.gov/nuccore/HF548531.1; KU641796, PpGS1b.2 cDNA https://www.ncbi.nlm.nih.gov/nuccore/KU641796; PpGS1b.2 gene allele 1 https://www.ncbi.nlm.nih.gov/nuccore/KU641799.1; PpGS1b.2 gene allele 2 https://www.ncbi.nlm.nih.gov/nuccore/KU641800.1].

DATA AVAILABILITY STATEMENT

Constructs are available from the corresponding authors upon request. The rest of the data supporting the findings of this study are available within the paper and within its supplementary materials published online.

REFERENCES

Afgan, E., Baker, D., Batut, B., van den Beek, M., Bouvier, D., Cech, M. *et al.* (2018) The Galaxy platform for accessible, reproducible and collaborative biomedical analyses: 2018 update. *Nucleic Acids Research*, **46**, W537–W544. Available from: https://doi.org/10.1093/nar/gky379

Aledo, J.C. (2021) Ptm: an R package for the study of methionine sulfoxidation and other post-translational modifications. *Bioinformatics*, **37**, 3979–3980. Available from: https://doi.org/10.1093/bioinformatics/btab348

Altschul, S.F., Gish, W., Miller, W., Myers, E.W. & Lipman, D.J. (1990) Basic local alignment search tool. *Journal of Molecular Biology*, **215**, 403–410. Available from: https://doi.org/10.1016/S0022-2836(05)80360-2

Ávila, C., Llebrés, M.T., Castro-Rodríguez, V., Lobato-FernÁndez, C., Reymond, I., Harvengt, L. *et al.* (2022) Identification of metabolic pathways differentially regulated in somatic and zygotic embryos of maritime pine. *Frontiers in Plant Science*, **13**, 877960. Available from: https://doi.org/10.3389/fpls.2022.877960

Ávila, C., Suárez, M.F., Gómez-Maldonado, J. & Cánovas, F.M. (2001) Spatial and temporal expression of two cytosolic glutamine synthetase

genes in scots pine: functional implications on nitrogen metabolism during early stages of conifer development. *The Plant Journal*, **25**, 93–102. Available from: https://doi.org/10.1046/j.1365-313x.2001.00938.x

Bao, A., Zhao, Z., Ding, G., Shi, L., Xu, F. & Cai, H. (2014) Accumulated expression level of cytosolic *glutamine synthetase 1* gene (*OsGs1;1* or *OsGS1;2*) alter plant development and the carbon-nitrogen metabolic status in rice. *PLoS One*, **9**, e95581. Available from: https://doi.org/10.1371/journal.pone.0095581

Bernard, S.M. & Habash, D.Z. (2009) The importance of cytosolic glutamine synthetase in nitrogen assimilation and recycling. *New Phytologist*, **182**, 608–620. Available from: https://doi.org/10.1111/j.1469-8137.2009.02823.x

Blackwell, R.D., Murray, A.J.S. & Lea, P.J. (1987) Inhibition of photosynthesis in barley with decreased levels of chloroplastic glutamine synthetase activity. *Journal of Experimental Botany*, **196**, 1799–1809. Available from: https://doi.org/10.1093/jxb/38.11.1799

Bolger, A.M., Lohse, M. & Usadel, B. (2014) Trimmomatic: a flexible trimmer for Illumina sequence data. *Bioinformatics*, **30**, 2114–2120. Available from: https://doi.org/10.1093/bioinformatics/btu170

Bradford, M.M. (1976) A rapid and sensitive method for the quantitation of microgram quantities of protein utilizing the principle of protein-dye binding. *Analytical Biochemistry*, **72**, 248–254. Available from: https://doi.org/10.1006/abio.1976.9999

Canales, J., Rueda-López, M., Craven-Bartle, B., Ávila, C. & Cánovas, F.M. (2012) Novel insights into regulation of asparagine synthetase in conifers. *Frontiers in Plant Science*, **3**, 100. Available from: https://doi.org/10.3389/fpls.2012.00100

Cañas, R.A., Canales, J., Gómez-Maldonado, J., Ávila, C. & Cánovas, F.M. (2014) Transcriptome analysis in maritime pine using laser capture microdissection and 454 pyrosequencing. *Tree Physiology*, **34**, 1278–1288. Available from: https://doi.org/10.1093/treephys/tpt113

Cañas, R.A., Canales, J., Muñoz-Hernández, C., Granados, J.M., Ávila, C., García-Martín, M.L. *et al.* (2015) Understanding developmental and adaptive cues in pine through metabolite profiling and co-expression network analysis. *Journal of Experimental Botany*, **66**, 3113–3127. Available from: https://doi.org/10.1093/jxb/erv118

Cañas, R.A., Li, Z., Pascual, M.B., Castro-Rodríguez, V., Ávila, C., Sterck, L. *et al.* (2017) The gene expression landscape of pine seedling tissues. *The Plant Journal*, **91**, 1064–1087. Available from: https://doi.org/10.1111/tpj.13617

Cánovas, F.M., Cantón, F.R., Gallardo, F., García-Gutiérrez, A. & de Vicente, A. (1991) Accumulation of glutamine synthetase during early development of maritime pine seedlings (*Pinus pinaster*). *Planta*, **185**, 372–378. Available from: https://doi.org/10.1007/BF00201059

Cantón, F.R., García-Gutiérrez, A., Crespillo, R. & Cánovas, F.M. (1996) High-level expression of *Pinus sylvestris* glutamine synthetase in *Escherichia coli*. Production of polyclonal antibodies against the recombinant protein and expression studies in pine seedlings. *FEBS Letters*, **393**, 205–210. Available from: https://doi.org/10.1016/0014-5793(96)00886-1

Cantón, F.R., Suárez, M.F., Josè-Estanyol, M. & Cánovas, F.M. (1999) Expression analysis of a cytosolic glutamine synthetase gene in cotyledons of scots pine seedlings: developmental, light regulation and spatial distribution of specific transcripts. *Plant Molecular Biology*, **404**, 623–634. Available from: https://doi.org/10.1023/a:1006219205062

Castro-Rodríguez, V., García-Gutiérrez, A., Cañas, R.A., Pascual, M.B., Ávila, C. & Cánovas, F.M. (2015) Redundancy and metabolic function of the glutamine synthetase gene family in poplar. *BMC Plant Biology*, **15**, 20. Available from: https://doi.org/10.1186/s12870-014-0365-5

de la Torre, F., García-Gutiérrez, A., Crespillo, R., Cantón, F.R., Ávila, C. & Cánovas, F.M. (2002) Functional expression of two pine glutamine synthetase genes in bacteria reveals that they encode cytosolic holoenzymes with different molecular and catalytic properties. *Plant and Cell Physiology*, **43**, 802–809. Available from: https://doi.org/10.1093/pcp/pcf094

De Smet, R. & Van de Peer, Y. (2012) Redundancy and rewiring of genetic networks following genome-wide duplication events. *Current Opinion in Plant Biology*, **15**, 168–176. Available from: https://doi.org/10.1016/j.pbi.2012.01.003

Edelheit, O., Hanukoglu, A. & Hanukoglu, I. (2009) Simple and efficient site-directed mutagenesis using two single-primer reactions in parallel to generate mutants for protein structure-function studies. *BMC Biotechnology*, **9**, 61. Available from: https://doi.org/10.1186/1472-6750-9-61

Edgar, R.C. (2004) MUSCLE: multiple sequence alignment with high accuracy and high throughput. *Nucleic Acids Research*, **32**, 1792–1797. Available from: https://doi.org/10.1093/nar/gkh340

Forde, B.G. (2014) Glutamate signalling in roots. *Journal of Experimental Botany*, **65**, 779–787. Available from: https://doi.org/10.1093/jxb/ert335

Forde, B.G. & Lea, P.J. (2007) Glutamate in plants: metabolism, regulation, and signaling. *Journal of Experimental Botany*, **58**, 2339–2358. Available from: https://doi.org/10.1093/jxb/erm121

Fujita, T., Beier, M.P., Tabuchi-Kobayashi, M., Hayatsu, Y., Nakamura, H., Umetsu-Ohashi, T. *et al.* (2022) Cytosolic glutamine synthetase GS1;3 is involved in rice grain ripening and germination. *Frontiers in Plant Science*, **13**, 835835. Available from: https://doi.org/10.3389/fpls.2022.835835

Funayama, K., Kojima, S., Tabuchi-Kobayashi, M., Sawa, Y., Nakayama, Y., Hayakawa, T. *et al.* (2013) Cytosolic glutamine synthetase 1;2 is responsible for the primary assimilation of ammonium in rice roots. *Plant and Cell Physiology*, **54**, 934–943. Available from: https://doi.org/10.1093/pcp/pct046

Gao, Y., de Bang, T.C. & Schjoerring, J.K. (2019) Cisgenic overexpression of cytosolic glutamine synthetase improves nitrogen utilization efficiency in barley and prevents grain protein decline under elevated CO_2. *Plant Biotechnology Journal*, **17**, 1209–1221. Available from: https://doi.org/10.1111/pbi.13046

Gawronski, J.D. & Benson, D.R. (2004) Microtiter assay for glutamine synthetase biosynthetic activity using inorganic phosphate detection. *Analytical Biochemistry*, **327**, 114–118. Available from: https://doi.org/10.1016/j.ab.2003.12.024

Gómez-Maldonado, J., Ávila, C., Barnestein, P., Crespillo, R. & Cánovas, F.M. (2004) Interaction of cist-acting elements in the expression of a gene encoding cytosolic glutamine synthetase in pine seedlings. *Physiologia Plantarum*, **121**, 537–545. Available from: https://doi.org/10.1111/j.1399-3054.2004.00353.x

Gómez-Maldonado, J., Cánovas, F.M. & Ávila, C. (2004) Molecular analysis of the 5′-upstream of a gibberellin-inducible cytosolic glutamine synthetase gene (*GS1b*) expressed in pine vascular tissue. *Planta*, **218**, 1036–1045. Available from: https://doi.org/10.1007/s00425-003-1185-2

Goodall, A.J., Kumar, P. & Tobin, A.K. (2013) Identification and expression analyses of cytosolic glutamine synthetase genes in barley (*Hordeum vulagre* L.). *Plant and Cell Physiology*, **54**, 492–505. Available from: https://doi.org/10.1093/pcp/pct006

Grabherr, M.G., Haas, B.J., Yassour, M., Levin, J.Z., Thompson, D.A., Amit, I. *et al.* (2011) Full-length transcriptome assembly from RNA-seq data without a reference genome. *Nature Biotechnology*, **29**, 644–652. Available from: https://doi.org/10.1038/nbt.1883

Granados, J.M., Ávila, C., Cánovas, F.M. & Cañas, R.A. (2016) Selection and testing of reference genes for accurate RT-qPCR in adult needles and seedlings of maritime pine. *Tree Genetic & Genomes*, **12**, 60–75. Available from: https://doi.org/10.1007/s11295-016-1018-7

Guan, M., Moller, I.S. & Schjoerring, J.K. (2015) Two cytosolic glutamine synthetase isoforms play specific roles for seed germination and seed yield structure in *Arabidopsis*. *Journal of Experimental Botany*, **66**, 203–212. Available from: https://doi.org/10.1093/jxb/eru411

Habash, D.Z., Massiah, A.J., Rong, H.L., Wallsgrove, R.M. & Leigh, R.A. (2001) The role of cytosolic glutamine synthetase in wheat. *Annals of Applied Biology*, **138**, 83–89. Available from: https://doi.org/10.1111/j.1744-7348.2001.tb00087.x

Hachiya, T., Inaba, J., Wakazaki, M., Sato, M., Toyooka, K., Miyagi, A. *et al.* (2021) Excessive ammonium assimilation by plastidic glutamine synthetase causes ammonium toxicity in *Arabidopsis thaliana*. *Nature Communications*, **12**, 4944. Available from: https://doi.org/10.1038/s41467-021-25238-7

Heldt, H. & Piechulla, B. (2011) *Plant Biochemestry*, fourth edition. San Diego: Academic Press, Elsevier.

Hirel, B. & Krapp, A. (2021) Nitrogen utilization in plants I biological and agronomic importance. In: Jez, J. (Ed.) *Encyclopedia of biological chemistry III*, Third edition. Amsterdam: Elsevier, pp. 127–140.

Ishiyama, K., Inoue, E., Tabuchi, M., Yamaya, T. & Takahashi, H. (2004) Biochemical background and compartmentalized functions of cytosolic glutamine synthetase for active ammonium assimilation in rice roots. *Plant and Cell Physiology*, **45**, 1640–1647. Available from: https://doi.org/10.1093/pcp/pch190

Ishiyama, K., Inoue, E., Watanabe-Takahashi, A., Obara, M., Yamaya, T. & Takahashi, H. (2004) Kinetic properties and ammonium-dependent regulation of cytosolic isoenzymes of glutamine synthetase in *Arabidopsis*. *The Journal of Biological Chemistry*, **279**, 16598–16605. Available from: https://doi.org/10.1074/jbc.M313710200

Ishiyama, K., Inoue, E., Yamaya, T. & Takahashi, H. (2006) Gln49 and Ser174 residues play critical roles in determining the catalytic efficiencies of plant glutamine synthetase. *Plant and Cell Physiology*, **47**, 299–303. Available from: https://doi.org/10.1093/pcp/pci238

James, D., Borphukan, B., Fartyal, D., Achary, V.M.M. & Reddy, M.K. (2018) Transgenic manipulation of glutamine synthetase: A target with untapped potential in various aspects of crop improvement. In: Gosal, S.S. & Wani, S.H. (Eds.) *Biotechnology of Crop Improvement*. Cham: Springer International Publishing AG, pp. 367–416.

Ji, Y., Li, Q., Liu, G., Selvaraj, G., Zheng, Z. & Wei, Y. (2019) Roles of cytosolic glutamine synthetase in *Arabidopsis* development and stress responses. *Plant and Cell Physiology*, **60**, 657–671. Available from: https://doi.org/10.1093/pcp/pcy235

Jones, D.T., Taylor, W.R. & Thornton, J.M. (1992) The rapid generation of mutation data matrices from protein sequences. *Computer Applications in the Biosciences*, **8**, 275–282. Available from: https://doi.org/10.1093/bioinformatics/8.3.275

Jumper, J., Evans, R., Pritzel, A., Green, T., Figurnov, M., Ronneberger, O. *et al.* (2021) Highly accurate protein structure prediction with AlphaFold. *Nature*, **596**, 583–589. Available from: https://doi.org/10.1038/s41586-021-03819-2

Kong, D., Ju, C., Parihar, A., Kim, S., Cho, D. & Kwak, J.M. (2015) *Arabidopsis* glutamate receptor homolog3.5 modulates cytosolic Ca^{2+} level to continue effect of abscisic acid in seed germination. *Plant Physiology*, **167**, 1630–1642. Available from: https://doi.org/10.1104/pp.114.251298

Lea, P.J. & Ireland, R.J. (1999) Nitrogen metabolism in higher Plants. In: Singh, B.K. (Ed.) *Plant Amino Acids*. New York: Marcel Dekker Inc, pp. 1–47.

Letunic, I. & Bork, P. (2019) Interactive tree of life (iTOL) v4: recent updates and new developments. *Nucleic Acids Research*, **47**, W256–W259. Available from: https://doi.org/10.1093/nar/gkz239

Levitzki, A. & Koshland, D.E., Jr. (1976) The role of negative cooperativity and half-of-the-sites reactivity in enzyme regulation. *Current Topics in Cellular Regulation*, **10**, 1–40. Available from: https://doi.org/10.1016/b978-0-12-152810-2.50008-5

Llorca, O., Betti, M., González, J.M., Valencia, A., Márquez, A.J. & Valpuesta, J.M. (2006) The three-dimensional structure of an eukaryotic glutamine synthetase: functional implications of its oligomeric structure. *Journal of Structural Biology*, **156**, 469–479. Available from: https://doi.org/10.1016/j.jsb.2006.06.003

López-Bucio, J.S., de la Cruz, H.R. & Guevara-García, A.A. (2019) Glutamate sensing in plants. In: Ramakrishna, A. & Roshchina, V.V. (Eds.) *Neurotransmitters in plants: perspectives and applications*. Raton: CRC Press, pp. 231–140.

Lothier, J., Gaufichon, L., Sormani, R., Lemaître, T., Azzopardi, M., Morin, H. *et al.* (2011) The cytosolic glutamine synthetase GLN1;2 plays a role in the control of plant growth and ammonium homeostasis in *Arabidopsis* rosettes when nitrate supply is not limiting. *Journal of Experimental Botany*, **62**, 1375–1390. Available from: https://doi.org/10.1093/jxb/erq299

Martin, A., Lee, J., Kichey, T., Gerentes, D., Zivy, M., Tatout, C. *et al.* (2006) Two cytosolic glutamine synthetase isoforms of maize are specifically involved in the control of grain production. *The Plant Cell*, **18**, 3252–3274. Available from: https://doi.org/10.1105/tpc.106.042689

Michard, E., Lima, P.T., Borges, F., Silva, A.C., Portes, M.T., Carvalho, J.E. *et al.* (2011) Glutamate receptor-like genes form Ca^{2+} channels in pollen tubes and are regulated by pistil D-serine. *Science*, **332**, 434–437. Available from: https://doi.org/10.1126/science.1201101

Mirdita, M., Schütze, K., Moriwaki, Y., Heo, L., Ovchinnikov, S. & Steinegger, M. (2022) ColabFold: making protein folding accessible to all. *Nature Methods*, **19**, 679–682. Available from: https://doi.org/10.1038/s41592-022-01488-1

Moreira, E., Coimbra, S. & Melo, P. (2022) Glutamine synthetase: an unlikely case of functional redundancy in *Arabidopsis thaliana*. *Plant Biology*, **24**, 713–720. Available from: https://doi.org/10.1111/plb.13408

Ortigosa, F., Lobato-Fernández, C., Shikano, H., Ávila, C., Taira, S., Cánovas, F.M. *et al.* (2022) Ammonium regulates the development of pine roots through hormonal crosstalk and differential expression of transcription factors in the apex. *Plant, Cell and Environment*, **45**, 915–935. Available from: https://doi.org/10.1111/pce.14214

Pérez-Rodríguez, M.J., Suárez, M.F., Heredia, R., Avila, C., Breton, D., Trontin, J.F. *et al.* (2005) Expression patterns of two glutamine synthetase genes in zygotic and somatic pine embryos support specific roles in nitrogen metabolism during embryogenesis. *New Phytologist*, **169**, 35–44. Available from: https://doi.org/10.1111/j.1469-8137.2005.01551.x

Qiu, X.M., Sun, Y.Y., Ye, X.Y. & Li, Z.G. (2020) Signaling role of glutamate in plants. *Frontiers in Plant Science*, **13**, 1743. Available from: https://doi.org/10.3389/fpls.2019.01743

Ritz, C. & Spiess, A.N. (2008) qpcR: an R package for sigmoidal model selection in quantitative real-time polymerase chain reaction analysis. *Bioinformatics*, **24**, 1549–1551. Available from: https://doi.org/10.1093/bioinformatics/btn227

Sakakibara, H., Shimizu, H., Hase, T., Yamazaki, Y., Takao, T., Shimonishi, Y. *et al.* (1996) Molecular identification and characterization of cytosolic isoforms of glutamine synthetase in maize roots. *The Journal of Biological Chemistry*, **271**, 29561–29568. Available from: https://doi.org/10.1074/jbc.271.47.29561

Schneider, W.L. & Gifford, D.J. (1994) Loblolly pine seed dormancy. I. the relationship between protein synthesis and the loss of dormancy. *Physiologia Plantarum*, **90**, 246–252. Available from: https://doi.org/10.1111/j.1399-3054.1994.tb00384.x

Shin, W.H., Lee, G.R., Heo, L., Lee, H. & Seok, C. (2014) Prediction of protein structure and interaction by GALAXY protein modeling programs. *BioDesign*, **2**, 1–11.

Sterck, L., de María, N., Cañas, R.A., de Miguel, M., Perdiguero, P., Raffin, A. *et al.* (2022) Maritime Pine Genomics in Focus. In: De La Torre, A.R. (Ed.) *The Pine Genomes*. Springer, Cham: Compendium of Plant Genomes, pp. 67–123.

Suárez, M.F., Ávila, C., Gallardo, F., Cantón, F.R., García-Gutiérrez, A.G., Claros, M.G. *et al.* (2002) Molecular and enzymatic analysis of ammonium assimilation in woody plants. *Journal of Experimental Botany*, **53**, 891–904. Available from: https://doi.org/10.1093/jexbot/53.370.891

Tabuchi, M., Sugiyama, K., Ishiyama, K., Inoue, E., Sato, T., Takahashi, H. *et al.* (2005) Severe reduction in growth rate and grain filling of rice mutants lacking *OsGS1;1* a cytosolic glutamine synthetase1;1. *The Plant Journal*, **42**, 641–651. Available from: https://doi.org/10.1111/j.1365-313X.2005.02406.x

Tamura, K., Stecher, G. & Kumar, S. (2021) MEGA11: molecular evolutionary genetics analysis version 11. *Molecular Biology and Evolution*, **38**, 3022–3027. Available from: https://doi.org/10.1093/molbev/msab120

Tegeder, M. & Masclaux-Daubresse, C. (2017) Source and sink mechanisms of nitrogen transport and use. *New Phytologist*, **217**, 35–53. Available from: https://doi.org/10.1111/nph.14876

Thomsen, H.C., Eriksson, D., Møller, I.S. & Schjoerring, J.K. (2014) Cytosolic glutamine synthetase: a target for improvement of crop nitrogen use efficiency? *Trends in Plant Science*, **19**, 656–663. Available from: https://doi.org/10.1016/j.tplants.2014.06.002

Tian, F., Yang, D.C., Meng, Y.Q., Jin, J. & Gao, G. (2020) PlantRegMap: charting functional regulatory maps in plants. *Nucleic Acids Research*, **48**, D1104–D1113. Available from: https://doi.org/10.1093/nar/gkz1020

Urriola, J. & Rathore, K.S. (2015) Overexpression of a glutamine synthetase gene affects growth and development in sorghum. *Transgenic Research*, **24**, 397–407. Available from: https://doi.org/10.1007/s11248-014-9852-6

Valderrama-Martín, J.M., Ortigosa, F., Ávila, C., Cánovas, F.M., Hirel, B., Cantón, F.R. *et al.* (2022) A revised view on the evolution of glutamine synthetase isoenzymes in plants. *The Plant Journal*, **110**, 946–960. Available from: https://doi.org/10.1111/tpj.15712

Varadi, M., Anyango, S., Deshpande, M., Nair, S., Natassia, C., Yordanova, G. *et al.* (2022) AlphaFold protein structure database: massively expanding the structure coverage of protein-sequence space with high-accuracy models. *Nucleic Acids Research*, **50**, D439–D444. Available from: https://doi.org/10.1093/nar/gkab1061

Villalobos, D.P. (2008) *Aproximación genómica al estudio de la formación de la madera en los pinos*. Universidad de Málaga, Málaga (Spain). Doctoral dissertation.

Wallsgrove, R.M., Turner, J.C., Hall, N.P., Kendall, A.C. & Bright, S.W.J. (1987) Barley mutants lacking chloroplast glutamine synthetase-

biochemical and genetic analysis. *Plant Physiology*, **83**, 155–158. Available from: https://doi.org/10.1104/pp.83.1.155

Wedler, F.C. & Horn, B.R. (1976) Catalytic mechanisms of glutamine synthetase enzymes. Studies with analogs of possible intermediates and transition states. *Journal of Biological Chemistry*, **251**, 7530–7538. Available from: https://doi.org/10.1016/S0021-9258(17)32883-1

Wei, Y., Xiong, S., Zhang, Z., Meng, X., Wang, L., Zhang, X. *et al.* (2021) Localization, gene expression, and functions of glutamine synthetase isoenzymes in wheat grain (*Trticum aestivum* L.). *Frontiers in Plant Science*, **12**, 580405. Available from: https://doi.org/10.3389/fpls.2021.580405

Wudick, M.M., Portes, M.T., Michard, E., Rosas-Santiago, P., Lizzio, M.A., Nunes, C.O. *et al.* (2018) CORNICHON sorting and regulation of GLR channels underlie pollen tube Ca^{2+} homeostasis. *Plant Science*, **360**, 533–536. Available from: https://doi.org/10.1126/science.aar6464

Yadav, S.K. (2009) Computational structural analysis and kinetic studies of a cytosolic glutamine synthetase from *Camellia sinensis* (L.) O. Kuntze. *Protein Journal*, **28**, 428–434. Available from: https://doi.org/10.1007/s10930-009-9210-3

Yamaya, T. & Kusano, M. (2014) Evidence supporting distinct functions of three cytosolic glutamine synthetases and two NADH-glutamate synthases in rice. *Journal of Experimental Botany*, **65**, 5519–5525. Available from: https://doi.org/10.1093/jxb/eru103

Zhao, W., Yang, J., Tian, Y., Fu, X., Zhu, B., Xue, Y. *et al.* (2014) Expression, purification, and characterization of recombinant mangrove glutamine synthetase. *Molecular Biology Reports*, **41**, 7575–7583. Available from: https://doi.org/10.1007/s11033-014-3649-9

Zhou, J.Y., Hao, D.L. & Yang, G.Z. (2021) Regulation of cytosolic pH: the contributions of plant plasma membrane H^+-ATPases and multiple transporters. *International Journal of Molecular Sciences*, **22**, 12998. Available from: https://doi.org/10.3390/ijms222312998